Estuaries and Coasts (2019) 42:470–493
https://doi.org/10.1007/s12237-018-0485-5

Is Submarine Groundwater Discharge (SGD) Important for the Historical Fish Kills and Harmful Algal Bloom Events of Mobile Bay?

Daniel Montiel[1] · Alexander Lamore[1] · Jackson Stewart[1] · Natasha Dimova[1]

Received: 2 August 2018 / Revised: 1 November 2018 / Accepted: 6 November 2018 / Published online: 19 November 2018

Abstract

Large-scale fish and crustacean kills, locally known as *Jubilees*, and harmful algal blooms (HABs) have been occurring in Mobile Bay (Alabama) for more than a century. In fact, the first record describing a *Jubilee* event in Mobile Bay during 1867 was the first ever-documented case of mass mortalities of marine animals caused by hypoxia. To evaluate the importance of submarine groundwater discharge (SGD) in the occurrence of *Jubilees* and HABs in Mobile Bay, a 3-year study was conducted using a multi-method approach. Significant spatial and temporal variations of SGD were revealed in the bay only by applying a combination of geochemical and shallow geophysical techniques. The development of seasonal hypoxia observed in bay waters in areas impacted by *Jubilees* was the result of anoxic SGD inputs, which magnitude and spatial distribution were controlled by shallow lithological heterogeneities created during the modern development of the bay. Although when compared to the river discharge SGD contributed between 0.2 (wet season) and 5% (dry season) of the total freshwater inputs to Mobile Bay, 80% of the total SGD in the bay occurred in areas ecologically impacted by hypoxia and *Jubilees*. In these areas, SGD comprised up to 37% of the total water inputs during the dry season, coinciding with the time of the year when *Jubilees* and HABs occur. In conclusion, while SGD might not be a significant source of fresh water to Mobile Bay or other estuaries worldwide, enhanced SGD caused by site-specific lithological heterogeneities can have a critical role in the development of hypoxia and ecological issues in nearshore waters.

Keywords Submarine groundwater discharge · Estuary · Lithologic heterogeneities · Hypoxia · Jubilees · Harmful algal blooms

Introduction

Submarine groundwater discharge (SGD) is a significant source of water and dissolved constituents in coastal environments worldwide (Johannes 1980; Moore 1999; Sawyer et al. 2014). However, in river-dominated coastal areas such as estuaries, SGD is typically overlooked due to its limited volumetric contribution compared to fluvial fluxes. Nevertheless, it has been demonstrated that SGD can rival riverine inputs in some areas, specifically with respect to material loadings (Moore 1996; Burnett and Dulaiova 2006; Xu et al. 2013). Understanding the coastal hydrogeology and consequent temporal and spatial variability of SGD is crucial for constructing local water budgets, adequately managing water resources, and studying the effects of SGD on estuarine ecosystems worldwide (Burnett et al. 2003; Henderson et al. 2010; Xu et al. 2013; Befus et al. 2014).

Estuaries are geologically dynamic transition systems, which geomorphology, water circulation, biogeochemistry, and ecology vary both temporally and spatially (Dyer 1973; Wolfe and Kjerfve 1986; Roman et al. 2000; Krantz et al. 2004). Modern estuaries were formed approximately 5000 years ago when the sea level reached its present level following the shoreline transgression and leading to estuarine-basin sediment accumulation comprised of different facies

Communicated by Isaac Santos

Electronic supplementary material The online version of this article (https://doi.org/10.1007/s12237-018-0485-5) contains supplementary material, which is available to authorized users.

✉ Daniel Montiel
dmontielmartin@crimson.ua.edu

Alexander Lamore
aflamore@crimson.ua.edu

Jackson Stewart
jbstewart4@crimson.ua.edu

Natasha Dimova
ntdimova@ua.edu

[1] Department of Geological Sciences, University of Alabama, Tuscaloosa 35487, USA

(Wolfe and Kjerfve 1986; Bianchi 2007; Rodriguez et al. 2010). These spatially diverse modern sediment deposits comprise the coastal shallow aquifers through which SGD often occurs (Krantz et al. 2004; Russoniello et al. 2013; Michael et al. 2016). Hydrogeological heterogeneities in combination with short- and long-term fluctuations of marine and terrestrial forcing, typical for coastal settings, result in high temporal and spatial variations of SGD in estuarine systems (Burnett et al. 2006; Santos et al. 2012; Russoniello et al. 2013; Uddameri et al. 2014). Due to this unique SGD variability, aerial thermal infrared (TIR) mapping of SGD or large-scale numerical modeling typically used in other coastal systems is not applicable to adequately evaluate SGD in estuaries (Stalker et al. 2009; Tamborski et al. 2015; Young et al. 2015).

The development of geochemical tracer techniques (e.g., radium and radon) during the last two decades has significantly advanced our ability to identify and quantify SGD in coastal zones worldwide (Moore 1996; Burnett et al. 2003). However, characterizing SGD in estuaries still bears a number of limitations and difficulties. For example, because estuarine basins receive water inputs from multiple sources (e.g., fluvial, marine, and groundwater) that vary seasonally, one of the challenges of using geochemical tracers mass-balances and mixing models is related to uncertainties in the determination of representative end-members (e.g., Xu et al. 2013; Rodellas et al. 2017; Cerdà-Domènech et al. 2017). In the coastal zone, SGD is comprised of terrestrially driven fresh groundwater (FSGD) and recirculated seawater (RSGD) controlled by marine forces (Taniguchi et al. 2005). Identifying and quantifying these two components are particularly important when constructing the fresh water budgets of coastal aquifers for water resources management efforts (Taniguchi et al. 2002; Null et al. 2012; Montiel et al. 2018). Typically, a salinity mixing model is used to address this task (Taniguchi et al. 2005; Charette 2007; Santos et al. 2009). However, in estuaries, salinity anomalies in the receiving surface waters are the result of both river and groundwater inputs. In these cases, applying a methodology approach based on multiple tracer techniques and shallow geophysics is imperative (Crusius et al. 2005; Tait et al. 2013).

Recent sensitivity analyses suggest that, in addition to the determination of the SGD end-members, the size of the seepage face bears the second largest uncertainty in radiotracers evaluations in the coastal zone (Montiel et al. 2018). For example, the direct output from the radon mass-balance modeling approach is groundwater specific discharge or Darcian's velocity (cm day^{-1}) (Burnet and Dulaiova 2003) and converting the radon-derived specific discharge to groundwater discharge (m^3 day^{-1}) requires constraining the size of the SGD plume area (m^2). This is often highly challenging because of the ephemeral nature of radon-gas and its fast mixing in these dynamic coastal systems (Lambert and Burnett 2003; Stieglitz et al. 2010). Similarly, when using the radium-based mass-balance approach, determining the volume of the tidal prism into which SGD takes place is usually difficult because the fresh groundwater tends to accumulate preferentially in the top layer of the water column (Garcia-Solsona et al. 2010; Tovar-Sanchez et al. 2014; Montiel et al. 2018).

The Mobile Bay Estuary in Alabama is located in the northern Gulf of Mexico to the east of the Mississippi River Delta (Fig. 1). Although this is the fourth largest estuary in the USA, groundwater contribution and hence its importance have never been studied before. However, previous studies have indicated that SGD might have significant effects on the coastal water quality with important economic and ecologic implications for this coastal region in the Gulf of Mexico (Stumpf et al. 1993; Bricker et al. 2008; Macintyre et al. 2011). During the summer, large-scale mortalities of fish and shellfish, locally known as *Jubilees*, have been observed in Mobile Bay for at least 150 years (Loesch 1960). Affected biota includes mainly demersal fish and crustaceans such as the blue crab, which are very valuable in this region (May 1973). These events have been attributed to water column stratification and oxygen depletion of bottom bay waters (May 1973; Turner et al. 1987). In addition to the *Jubilee* events, harmful algal blooms (HABs) have been reported in the southern area of Mobile Bay where river inputs are limited (Parsons and Dortch 2002; Liefer et al. 2009; Mcintyre et al. 2011; Su et al. 2014). As of now, the direct causes of these two phenomena remain poorly understood.

In this study, we investigated the role of SGD on the occurrence of *Jubilees* and HABs in Mobile Bay during 3 consecutive years (2015–2017). We assessed the importance of SGD to the water budget of Mobile Bay, including the areas affected by these events. We used a combination of radiotracer techniques (^{226}Ra, ^{224}Ra, ^{223}Ra, and ^{222}Rn), stable isotopes ($\delta^{18}O$ and $\delta^{2}H$), and seepage meter deployments during 3 consecutive years (2015–2017). To understand the SGD flow paths in the heterogeneous shallow aquifer and the potential effect on Jubilee and HAB events, we measured dissolved oxygen (DO) in groundwater and surface waters, conducted shallow geophysical surveys using both land-based (electrical resistivity tomography, ERT) and marine-borne (continuous resistivity profiling, CRP) resistivity measurements, and collected sediment cores in ecologically impacted areas.

Research Area

Mobile Bay is a shallow (av. depth of 3.5 m) estuary with a total area of 1315 km^2. The bay exchanges water with the Gulf of Mexico mainly through Main Pass between Dauphin Island and Morgan Peninsula (Greene et al. 2007; Rodriguez et al. 2008) (Fig. 1).

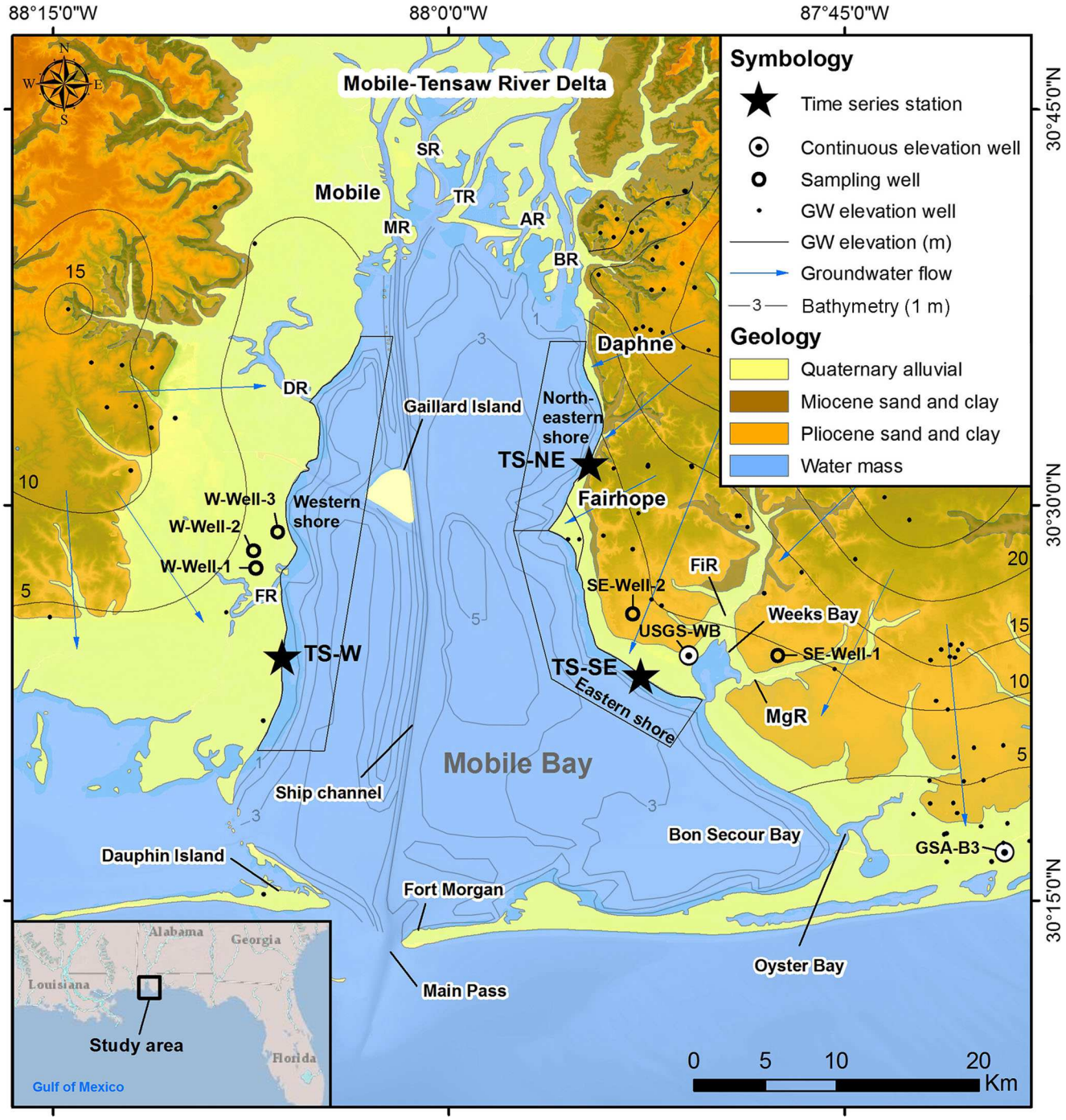

Fig. 1 Research area location and hydrogeological map showing the potentiometric surface of the Miocene-Pliocene Aquifer (data from the Geological Survey of Alabama), groundwater flow direction, monitoring wells for groundwater elevation, and sampled wells. The map includes the estuary bathymetry isolines in 1-m intervals (NOAA). The research area is divided in three sections: western shore, northeastern shore, and southeastern shore. At each section, the study sites where ERT lines, sediment core sampling, piezometers installation (Pz-1 to Pz-5), radon time series, radium assessments, and seepage meter deployments were conducted are represented with a star. The locations of Fowl River (FR), Dog River (DR), Mobile River (MR), Spanish River (SR), Tensaw River (TR), Apalachee River (AR), Blakeley River (BR), Fish River (FiR), and Magnolia River (MgR) are also indicated on the map

The climate of coastal Alabama is humid subtropical with annual precipitation of 1670 mm year^{-1} and an average temperature of 21 °C. Rainfall is highly variable throughout the year with a maximum during March and August and minimum during June and October (Ward et al. 2005).

The primary source of runoff into Mobile Bay (~95%) is the Mobile-Tensaw River System, which is comprised of five rivers at the Mobile-Tensaw River Delta: the Mobile, Spanish, Tensaw, Apalachee, and Blakeley Rivers. The average discharge of the system is 1500×10^5 m^3 day^{-1} with a strong seasonal pattern that can differ considerably from year to year (Schroeder 1978; Dzwonkowski et al. 2011). The peak of the river discharge occurs during March coinciding with the highest precipitation, whereas minimum discharge is from July to September (Schroeder et al. 1990; Ward et al. 2005). Discharge from the Mobile-Tensaw River System is the primary control on the water circulation and residence time in Mobile Bay. However, the flushing rates and salinity variations within the bay are also affected by the interplay of several natural and anthropogenic factors including: prevailing westerly winds during fall/winter and easterly winds during spring/summer, the diurnal tidal cycle (average range is 0.4 m), groundwater inputs, and the presence of a ship channel (Fig. 1) dredged frequently to maintain a depth of 15 m (Byrnes et al. 2013; Webb and Marr 2016; Du et al. 2018).

The coastal geology of the east and west shores of Mobile Bay consists of a Miocene to Holocene sequence of sand strata interbedded by clay layers (Gillett et al. 2000). This configuration comprises the shallow lithology (up to 300 m) and the hydrogeological settings of the Mobile Bay shoreline. Previous studies have suggested that groundwater discharge to Mobile Bay must occur through two principal aquifer units comprised of highly heterogeneous deposits: the Watercourse and the Miocene-Pliocene Aquifers (Walter and Kidd 1979; Gillett et al. 2000). The Watercourse Aquifer (referred as A1 in the literature) is the upper unconfined unit comprised of Pleistocene to Holocene alluvial and coastal deposits with a maximum thickness of 20 m that is only present in the southern sector of both the west and east shores of Mobile Bay. The Miocene-Pliocene Aquifer is divided into two sandy aquifer units: a shallow semi-confined Pliocene aquifer unit (A2) with thickness of 50–60 m and a Miocene confined aquifer unit (A3) with a thickness of 100–300 m. Aquifer unit A3 is hydraulically disconnected from unit A2 and Mobile Bay. Aquifer unit A2 of the Miocene-Pliocene Aquifer is hydraulically connected with Mobile Bay along both the west and east shores (Reed 1971; Chandler et al. 1985; Gillett et al. 2000; Ellis 2013).

Methods

In order to evaluate whether SGD can affect the occurrence of *Jubilees* and HABs in Mobile Bay, we identified and quantified SGD along the shoreline of the bay, focusing particularly on the ecologically impacted locations.

To facilitate this study, we formally divided the Mobile Bay coastline into three sections based on their shallow geologic make up, similarity in near-shore hydraulic gradients, and preliminary surface water tracer data. Hereinafter, we will refer to them as the (1) *western shore*, (2) *southeastern shore*, and (3) *northeastern shore* (Fig. 1). At each of these sections, we had a study site (i.e., TS-W, TS-SE, and TS-NE) where we conducted parallel research for comparison purposes.

Surface Water End-Member Characterization

To characterize the Mobile Bay waters end-member, we conducted boat surveys at a constant speed of 2–4 km h^{-1} along the shoreline and across Mobile Bay collecting continuous measurements for DO, conductivity, temperature, ^{222}Rn concentrations, and discrete samples for radium isotopes (^{223}Ra, ^{224}Ra, and ^{226}Ra) and stable isotopes ($\delta^{18}O$ and $\delta^{2}H$). We repeated these surveys five times, three times during the wet season (March of 2015, March 2016, and July 2017) and twice during the dry season (July of 2015 and March 2017). During all sampling campaigns, DO, conductivity, and temperature were measured continuously at 1-min intervals in conjunction with GPS positioning (Lowrance HDS 5) with an accuracy of ± 1 m. DO in surface water and groundwater was measured using a Pro2030 (YSI, Inc.) handheld instrument with a Galvanic sensor and a 1.25 mil polyethylene membrane with an accuracy of ± 0.2 mg L^{-1}. Before sampling, the DO sensor was calibrated following the YSI calibration procedure. Temperature and conductivity were measured using a conductivity-temperature-depth sensor (CTD, Solinst®) with accuracies of ± 20 μS cm^{-1} and ± 0.1 °C. Salinity values were calculated from CTD readings using the conversion method 2520B (APHA 1999) with an error of ± 0.1. Radon-222 concentrations in surface waters were measured in 10-min intervals using a RAD7 (Durridge Co., Inc.) portable radon-in-air monitor with a RAD AQUA accessory from a depth of 0.3 m. A detailed description of the survey procedure and RAD7 operation can be found elsewhere (Dulaiova et al. 2005; Dimova et al. 2009). To be able to compare all radon surveys and identify areas with temporally constant peaks of ^{222}Rn concentrations, all radon values in surface waters were normalized to the mean value during each survey. Thus, data presented here is reported also as ^{222}Rn anomalies, defined as positive or negative deviations from the mean. The surface water ^{222}Rn end-members at each study site (i.e., TS-W, TS-SE, and TS-NE) were determined by collecting time-series measurements in 30-min intervals (0.5 and 5 days) using a RAD AQUA set up, with uncertainties (1σ) of 5–10%. (Fig. 1) (Burnett and Dulaiova 2003).

Concentrations of radium isotopes in bay surface water were evaluated by collecting 120-L samples from a depth of 0.5 m. Samples were filtered through a PVC column filled with 20 g (dry weight) of MnO_2-coated-fibers (Mn-fibers) at a flow rate of approximately 1 L min^{-1} to ensure quantitative radium absorption (Moore 1976, 2008). Short-lived radium

isotopes (^{224}Ra and ^{223}Ra) were measured using a RaDeCC (radium delayed coincidence counter) system according to Moore and Arnold (1996), Sun and Torgersen (1998), and Garcia-Solsona et al. (2008). Radium-226 concentrations and uncertainties were measured using the RaDeCC-based method described in Geibert et al. (2013).

Water stable isotopes (δ^{18}O and δ^{2}H) in surface bay water were filtered with sterile 0.45-μm cellulose acetate filters and collected in 40-mL vials and were analyzed at the UC Davis Stable Isotopes Facility using a laser spectrometer (Water Isotope Analyzer V2, Los Gatos Research, Inc.) with accuracies of ± 1 and ± 0.1‰ for δ^{2}H and δ^{18}O, respectively. Isotopic ratios were calculated using the Vienna Standard Mean Ocean Water (VSMOW, in ‰).

To characterize the river surface water end-member, samples were collected during all sampling campaigns from the Mobile-Tensaw River Delta from Mobile, Tensaw, Apalachee, and Blakeley Rivers at their point of discharge to the bay. The seawater end-member was characterized using samples collected in Dauphin Island representative of the Gulf of Mexico waters entering the bay through Main Pass. DO, radium isotopes, and stable isotopes in river and seawater end-members were measured following the same procedures and methodologies as for Mobile Bay surface waters. Conductivity, salinity, and temperature were measured using a Pro2030 (YSI, Inc.) handheld meter with accuracies of ± 1 μS cm^{-1}, ± 0.1, and ± 0.3 °C.

Groundwater End-Member Characterization

To characterize the groundwater end-member at each study site (TS-W, TS-SE, and TS-NE), DO, temperature, salinity, water stable isotopes (δ^{18}O and δ^{2}H), and radioisotopes (^{222}Rn, ^{223}Ra, ^{224}Ra, and ^{226}Ra) were measured in groundwater from preexisting inland wells and shore-perpendicular transects of piezometers installed at the shore during this study. The shore-perpendicular transects consisted of five piezometers (Pz-1 to Pz-5) installed at different depths (Fig. 1). At all three study sites, piezometers Pz-1 were located 20-m inland from the mid-tidal line; Pz-2 and Pz-3 were placed 10-m away from the shoreline; piezometers Pz-4 were installed at the high tide mark, and piezometer Pz-5 were placed at the low tide mark. From land to offshore, the piezometers were screened at 4 (Pz-1), 1.5 (Pz-2), 1 (Pz-3), 1 (Pz-4, at the high tide mark), and 1 m (Pz-5, at the low tide mark) depths to include the subsurface mixing zone, i.e., the saltwater-fresh groundwater interphase. Additionally, during July of 2017, a 2-m multi-level piezometer (SE-Pz-4.5) was installed at study site TS-SE. Using this setup, we were able to recover pore water from six ports of the multiple-point sampler at 0.3-m depth intervals. Groundwater was also collected from five deeper wells (screen depth between 10 and 12 m), which were installed farther inland both in the west shore (W-Well-1, W-Well-2, W-Well-3) and the east shore (SE-Well-1 and SE-Well-2) of Mobile Bay (Fig. 1). In all cases, the radon groundwater end-member was measured with the RAD H_2O system (Durridge, Inc.) using 250-mL duplicates, typically with uncertainties of 10–20%. Radium isotopes and stable isotopes in groundwater were measured following the same procedure and methodologies as described for surface water end-members but using 20 L for radium samples. Similarly to the river end-member, groundwater DO, conductivity, salinity, and temperature were also measured using the Pro2030 (YSI, Inc.) handheld meter.

Shallow Aquifer Characterization

Five boat surveys employing streaming CRP measurements were conducted using an AGI SuperSting R8 Marine (AGI, Inc.) resistivity meter connected to a 33-m floating streamer (11 electrodes with 3-m spacing), which was towed from a boat. Continuous measurements were collected in a dipole-dipole configuration, which allowed a total penetration depth (water column and depth below the sediment-water interface) of 7 m. To inspect the hydrogeological properties of the SGD-saturated shallow sediments, electrical resistivity data from the same depth (5–7 m) during all surveys were extracted and combined to create an integrated one-dimensional map. Land-based shore-perpendicular ERT measurements were conducted at each study site (TS-W, TS-SE, and TS-NE) using a 168-m cable (56 electrodes with 3-m spacing) in a dipole-dipole configuration, which resulted in a sediment penetration depth up to 35 m. To monitor changes in the size of the SGD plume area due to tidal forcing, we performed time-lapsed ERT measurements at each site during falling tide. Data from both CRP and ERT were processed and interpreted using EarthImager 2D software (AGI, Inc.). The root mean square error (RMS) and L2-norm (sum of the squared weighted data errors) were used as data quality criteria for all measurements (Advanced Geosciences Inc. 2014). The detailed data processing procedures can be found in Cross et al. (2013) and Dimova et al. (2012).

During the installation of the deepest piezometers at each study site (i.e., piezometers Pz-1), we recovered individual sediment cores using a Geoprobe coring system (Model 5410, Geoprobe Systems Inc.). These three cores (from each study site) were brought to the lab and sectioned in 5-cm intervals for density, porosity, and grain size analysis following the procedure described in Lambe (1951). Grain size was determined using decreasing pore size (2.36 to 0.038 mm) stacked sieves (Fisher Scientific USA standard). Sediments were classified based on the Wentworth scale (Wentworth 1922). The hydraulic conductivity of each sediment type was estimated applying the Hazen approximation (Hazen 1893). Organic matter content of each sample was obtained following the ASTM 2974-87 methodology via mass

differential after combustion at 550 °C (American Association for Testing and Materials 1993).

SGD Assessments and Mobile Bay Water Budget

To evaluate total SGD (combined FSGD and RSGD), site-specific ^{222}Rn mass balances (Eqs. S1, S2, and S3) were constructed during wet (March of 2015 and 2016, and July 2017) and dry seasons (July of 2015, June of 2016, and March 2017). Descriptions of the radon mass-balance modeling approach can be found elsewhere (Cable et al. 1996; Burnett and Dulaiova 2003; Burnett et al. 2008). During June of 2016, total SGD was also evaluated using Lee-type seepage meters (Lee 1977) that were deployed at all three study sites (Eq. S4).

To assess the recirculated brackish SGD (RSGD), a three-end-member mixing model was used based on ^{224}Ra and ^{226}Ra activities (e.g., Hwang et al. 2005; Gu et al. 2012) measured in the three end-members, i.e., (1) Mobile-Tensaw River System, (2) seawater, and (3) RSGD, entering Mobile Bay (Eqs. S5, S6, S7, and S8) (Null et al. 2012; Moore 2003; Young et al. 2008). In addition to the radium approach, we also utilized two-end-member mixing models (Eqs. S10 and S11) based on the water stable isotopes δ^{18}O and δ^{2}H to evaluate the FSGD and RSGD components of the total SGD at of each study site following an approach described by Taniguchi et al. (2005).

Finally, the water budget of Mobile Bay was calculated using a three-end-member mixing model (Eqs. S12, S13, and S14) based on the water stable isotopes (δ^{18}O and δ^{2}H) (Doctor et al. 2006).

Results

Water End-Members

Surface Water End-Members

During the three-year study, ^{222}Rn concentrations in Mobile Bay waters (Mobile Bay end-member) were measured during boat surveys and continuous time-series. During all surveys, radon was always highest at both the northeastern and southeastern shores (study sites TS-NE and TS-SE) with positive anomalies of 0.8–5.0 × 10^3 and 0.1–5.0 × 10^3 dpm m^{-3}, respectively (Fig. 2a). Another persistent positive anomaly of 0.4–1.5 × 10^3 dpm m^{-3} was detected on the north end of the western shore. The ^{222}Rn concentrations in the rest of the western shore, Bon Secour Bay, and mid-bay waters presented negative anomalies of − 4.1–0.0 × 10^3 dpm m^{-3} (Fig. 2a). During all ^{222}Rn time-series measurements, the temporal average surface water end-members were 4.7 ± 1.3 × 10^3 (n = 353), 6.2 ± 1.0 × 10^3 (n = 754), and 8.3 ± 2.2 × 10^3 dpm m^{-3} (n = 1191) at study sites TS-W, TS-SE, and TS-NE, respectively.

DO in Mobile Bay was on average 4.1 ± 1.4 mg L^{-1} (n = 88) (Fig. S1). The highest DO values were measured near the river delta and Main Pass with concentrations of 6–8 mg L^{-1}, whereas along the east shore of the bay DO was always below 2 mg L^{-1} (Fig. S1). Salinity in the bay was on average 4.2 ± 3.2 during dry season and 1.7 ± 1.8 during the wet season (Fig. S2). Water stable isotopes ($\delta^{2}H_{MB}$ and $\delta^{18}O_{MB}$) in bay waters were between − 11 ± 3 and − 2.2 ± 0.8‰ (n = 30) during dry seasons and − 20 ± 4 and − 3.8 ± 0.5‰ (n = 41) during wet seasons. Radium concentrations in Mobile Bay waters were on average 200 ± 20 (^{226}Ra), 170 ± 10 (^{224}Ra), and 7 ± 1 dpm m^{-3} (^{223}Ra) (n = 32) during dry seasons. During wet seasons, the average concentrations were 150 ± 20 (^{226}Ra), 90 ± 5 (^{224}Ra), and 4 ± 1 dpm m^{-3} (^{223}Ra) (n = 29) (Table S1, Figs. S3a and S3b). The residence time (t) in Mobile Bay, calculated using Eq. S9, showed similar spatial distributions during both the dry and wet seasons, with averages of 7.0 ± 3.5 and 5.1 ± 2.5 days and maximum values of 8.1 and 13.9 days in the southeastern shore and Bon Secour Bay (Fig. 3a, b).

DO in the Mobile-Tensaw River System waters was on average 7.0 ± 1.8 mg L^{-1} (n = 18), while salinity was always below 0.4 (i.e., fresh) during all sampling campaigns (Table S1). The average water stable isotopes in the river system ($\delta^{2}H_{River}$ and $\delta^{18}O_{River}$) during wet seasons were − 18 ± 3 and − 3.5 ± 0.2‰ (n = 8) and − 15 ± 2 and − 3.0 ± 0.5‰ (n = 13) during dry seasons (Fig. 4). The average radium concentrations (Ra_{River}) were 150 ± 10 (^{226}Ra), 50 ± 3 (^{224}Ra), and 3.0 ± 0.2 dpm m^{-3} (^{223}Ra) (n = 7), respectively (Table S1).

The average salinity in the Gulf of Mexico's seawater end-member offshore of Dauphin Island was 25.8 ± 1.0 and the water stable isotopes ($\delta^{2}H_{ow}$ and $\delta^{18}O_{ow}$) values were 0.2 and 0.0 (n = 3), both in the range of marine environments (Fig. 4). Radium end-members in the Gulf seawater (Ra_{ow}) were on average 40 ± 5 (^{226}Ra), 20 ± 3 (^{224}Ra), and 1 ± 0.2 dpm m^{-3} (^{223}Ra) (n = 4) during dry seasons and 50 ± 7 (^{226}Ra), 40 ± 6 (^{224}Ra), and 2 ± 0.5 dpm m^{-3} (^{223}Ra) (n = 4) during rainy seasons (Table S1).

Groundwater End-Members

On the western shore at study site TS-W, the ^{222}Rn groundwater end-member (Rn_{SGD}) measured in the piezometer transect installed on the beach (W-Pz-1 to W-Pz-3) was 320 ± 40 × 10^3 dpm m^{-3} on average (n = 3). Radium concentrations were 6610 ± 330 (^{226}Ra), 1130 ± 100 (^{224}Ra), and 30 ± 2 dpm m^{-3} (^{223}Ra) (n = 1). DO was on average 1.2 ± 0.2 mg L^{-1} (n = 3) in the inland wells (W-Well-1, W-Well-2, and W-Well-3), whereas in the intertidal piezometers (W-Pz-1 to W-Pz-5) DO was 1.2–2.4 mg L^{-1} (n = 14) during all

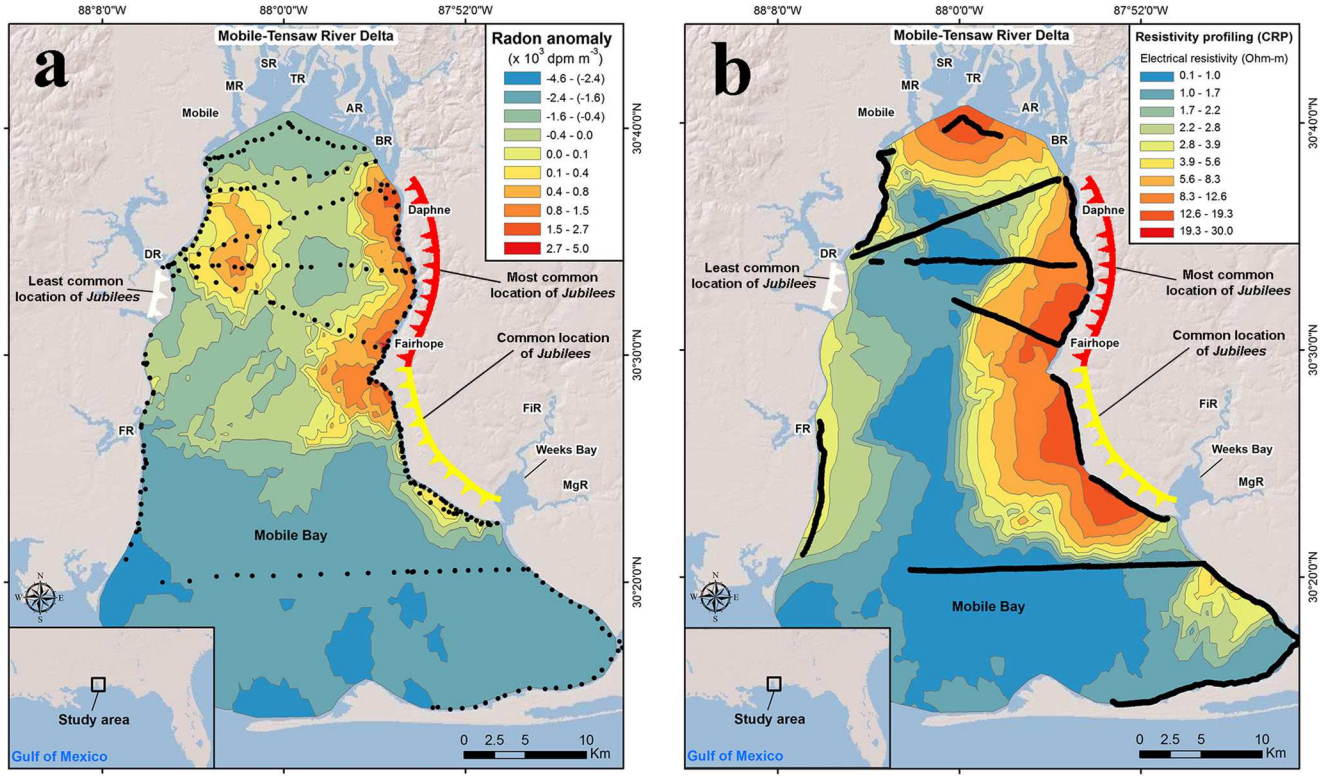

Fig. 2 **a** Distribution map of ^{222}Rn anomaly surveys on Mobile Bay surface water. The highest ^{222}Rn positive anomalies were found along the northeastern shore (0.8–5.0 × 10^3 dpm m^{-3}) and the southeastern shore (0.1–5.0 × 10^3 dpm m^{-3}). A positive anomaly (0.4–1.5 × 10^3 dpm m^{-3}) of lower magnitude was also detected in the northern sector of the western shore. Along the western shore, Bon Secour Bay, and Mid-Bay the ^{222}Rn concentrations were always lower resulting in negative anomalies (− 4.1–0.0 × 10^3 dpm m^{-3}). **b** Continuous resistivity profiling (CRP) surveys conducted in Mobile Bay depicting electrical resistivity at a depth of 5–7 m. The highest resistivity values (12–30 Ohm m) were found along the northeastern and southeastern shores. Higher resistivity was also measured near the delta where river fresh water inputs occur. Both panels (**a** and **b**) show the locations where *Jubilees* occur in Mobile Bay based on Loesch (1960) and May (1971) and inspired on a figure created by Paul Fehler

sampling campaigns (Fig. 5). The average salinity of groundwater at study site TS-W ranged from 2.1 to 5.7 during wet and dry seasons, respectively (Table S1). Average water stable isotopes δ^2H and δ^{18}O values were − 9 and − 2.1‰ (n = 6) during dry seasons and − 16 and − 3.4‰ during wet seasons (n = 5) (Fig. 4).

On the southeastern shore of Mobile Bay at study site TS-SE, the ^{222}Rn groundwater end-member (Rn_{SGD}) was 50 ± 10 × 10^3 dpm m^{-3} (n = 6). Radium concentrations (Ra_{SGD}) were on average 520 ± 30 (^{226}Ra), 410 ± 30 (^{224}Ra), and 10 ± 1 dpm m^{-3} (^{223}Ra), respectively (n = 2). DO was on average 5.6 ± 0.7 mg L^{-1} (n = 6) in the inland wells (SE-Well-1 and SE-Well-2), while in the intertidal piezometers (SE-Pz-1 to SE-Pz-5) DO was 0.8 ± 0.7 mg L^{-1} (n = 27) (Fig. 5). The average salinity in groundwater at the TS-SE site ranged from 2.3 to 5.8 during wet and dry seasons, respectively (Table S1). Average δ^2H and δ^{18}O values (δ^2H_{SGD}-$\delta^{18}O_{SGD}$) ranged between − 11 and − 2.5‰ during dry seasons and − 17 and − 3.8‰ during wet seasons (Fig. 4).

On the northeastern shore of Mobile Bay at study site TS-NE, the ^{222}Rn groundwater end-member (Rn_{SGD}) was 60 ± 20 × 10^3 dpm m^{-3} (n = 8). Radium concentrations (Ra_{SGD}) were 540 ± 50 (^{226}Ra), 480 ± 40 (^{224}Ra), and 12 ± 1 dpm m^{-3} (^{223}Ra), respectively (n = 3). Groundwater DO was on average 2.2 ± 1.0 mg L^{-1} (n = 19) in all intertidal piezometers (NE-Pz-1 to NE-Pz-5) (Fig. 5). The average salinity ranged from 1.0 to 2.8 during wet and dry seasons, respectively (Table S1). Average δ^2H and δ^{18}O values (δ^2H_{SGD}-$\delta^{18}O_{SGD}$) ranged between − 17 and − 3.6‰ during dry seasons and − 20 and − 4.1‰ during wet seasons (Fig. 4).

Shallow Aquifer Properties

Continuous Resistivity Profiling

CRP boat surveys revealed resistivity values for SGD-saturated shallow sediments (5–7-m depth) between 12 and 30 Ohm m along the southeastern and northeastern shores, with maximum values of 890 and 40 Ohm m near study areas TS-NE and TS-SE, respectively. Near the river delta, we found resistivity values up to 30 Ohm m. Along the western shore, resistivity values were between 2.8 to 5.6 Ohm m, with

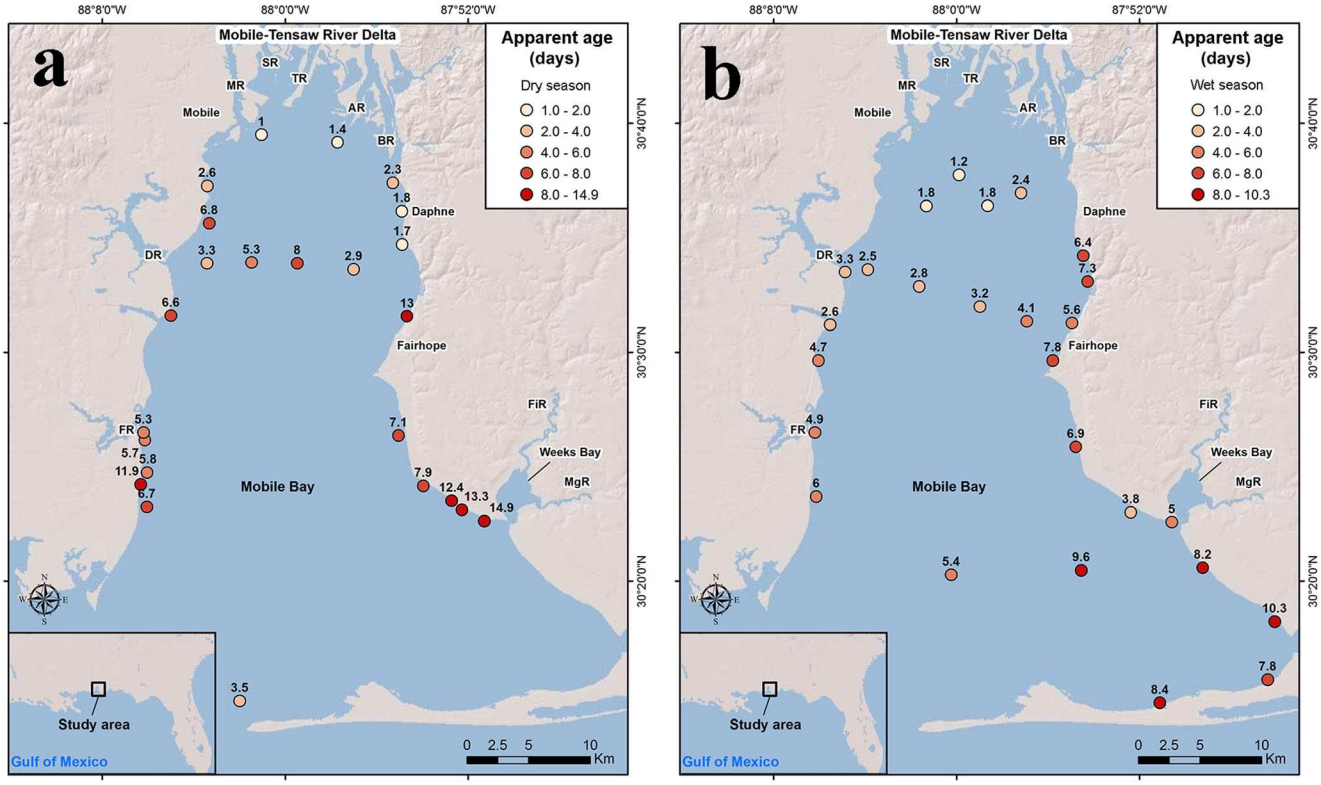

Fig. 3 Apparent water ages of Mobile Bay waters during the dry (**a**) and wet (**b**) seasons based on ^{223}Ra and Ra^{224} activity ratios. The highest water residence times were found on the southeastern shore and Bon Secour Bay, while the lowest values were found near the Mobile-Tensaw Delta and in the Mid Bay area. During dry season when river discharge was lowest, the overall residence time of the bay was higher (7.0 ± 3.5 days) compared to the wet seasons (5.1 ± 2.5 days)

a maximum of 10 Ohm m near study site TS-W (Fig. 2b). CRP transects conducted in the mid-bay area revealed resistivity values between 0.1 and 2.8 Ohm m (Fig. 2b).

Electrical Resistivity Tomography

To determine the size of the SGD plume area and characterize the shallow aquifer, land-based ERT was conducted at all three study sites. In all cases, the cable was placed perpendicular to the shore (i.e., parallel to the five-piezometer transect) with about two thirds of the cable submerged under water. To eliminate lithological interferences in the interpretation of the seepage area dimensions, in all study sites, we ran time-lapsed ERT measurements (total of three measurements per site) at a fixed location during falling tide.

On the western shore (study site TS-W), we identified three distinctive sediment strata (Fig. 6a). From top to bottom these are: (A) a shallow layer with average resistivity 10 Ohm m found to be present throughout the 2D line; (B) a medium layer with resistivity values of 1–3 Ohm m present from Pz-1 into the bay, and (C) a bottom layer that extends vertically to the full penetration depth with resistivity values between 8 and 35 Ohm m. During falling tide, we found that the SGD plume extended about 80 m into the Bay within the bottom layer (C) (Figs. 6a and S4a).

The ERT measurements conducted in the southeastern and northeastern shore (study sites TS-SE and TS-EN) indicated similar offshore stratigraphy with a sequence of horizontal sediment layers following the same pattern. At study site TS-SE, (A) a shallow sediment layer is present on the surface up to ~ 60 m from the shore with an electrical resistivity of about 10 Ohm m. Underlying this shallow layer (B), we identified a sediment deposit with resistivity values of 1–3 Ohm m. Up to the total depth of penetration, we found a thick sediment layer (C-D) with resistivity values that varied from 10 to 100 Ohm m. During time-lapsed ERT measurements, we found a groundwater plume extending up to 70 m offshore during the lowest tide stage in the deeper layer (C–D) (Figs. 6b and S4b). At study site TS-NE, we found a similar stratigraphy as at study site TS-SE. However, at the land side of the groundwater-seawater mixing zone, we identified a high resistivity layer (E) of > 100 Ohm m, which was not present in study site TS-SE. These high resistivity values were associated with coarse beach sand that extend about 20 m into the bay where it was in contact with sediment layers A, B, C, and D, following the same sequence as in TS-SE. During falling tide, we observed that the size of the SGD plume

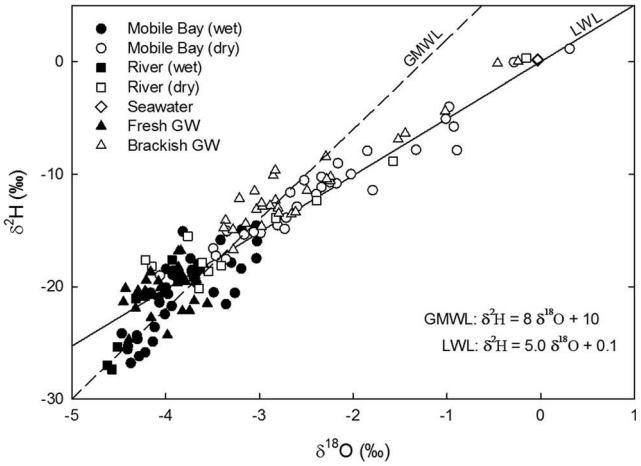

Fig. 4 Isotopic composition (δ^2H and $\delta^{18}O$) of water samples collected in Mobile Bay (Mobile Bay), Mobile-Tensaw River System (River), seawater from the Gulf of Mexico (Seawater), fresh groundwater (Fresh GW), and brackish groundwater (Brackish GW). Surface water samples (Mobile Bay and rivers) collected during the wet season (wet) are represented with closed symbols, and samples collected during the dry season (dry) are shown as open symbols. Fresh groundwater samples (closed symbols) were collected from inland wells W-Well-1 and W-Well-2 on the western shore, wells SE-Well-1, SE-Well-2, and SE-Well-3 on the east shore and piezometers Pz-1 and Pz-2 at all three study sites. Brackish groundwater samples (open symbols) were collected from piezometers Pz-3 to Pz-3 at all three study sites. The Local Water Line (LWL) represents the linear trend based on all water samples collected in the study area and the Global Meteoric Water Line (GMWL) is based on Craig (1961)

(observed in the coarse sand layer E and deeper layer D) reached 100 m offshore during the lowest tide stage (Figs. 6c and S4c). We used the plume dimensions measured during the lowest tide stage at the three study sites to calculate the SGD seepage face.

Shallow Coastal Sediment Characteristics

To constrain the geologic interpretation from the ERT measurements at each study site, we collected a total of three sediment cores (one per study site) at the intertidal zone and performed sediment analyses (Figs. S4a, S4b, and S4c). Grain size analyses, density, porosity, organic matter content, and hydraulic conductivity of all sediment layers can be found in Table 1.

On the western shore, consistently with the ERT images, sediment analyses of core TS-W revealed a three-layer structure with: layer (A) up to 0.8 m comprised of medium to coarse sand with a hydraulic conductivity of 10.5 m day^{-1}, layer (B) between 0.8 and 3.5 m was identified as gray coarse silt to very fine sand deposit with 11% of organic matter and a hydraulic conductivity of 4.1 m day^{-1}, and layer (C) at depth between 3.5 and 4 m was mostly olive-gray medium to fine sand with a hydraulic conductivity of 7.9 m day^{-1} (Figs. S4a and 6a). Based on the stratigraphic data reported in Gillett et al. (2000), layer C most likely corresponds with the Middle Sand formation within the Miocene-Pliocene Aquifer.

On the southeastern, the sediment core TS-SE presented four distinct layers, from top to bottom. These are (A) a 0.5-m white quarzitic medium to coarse sand with a hydraulic conductivity of 11.5 m day^{-1}; (B) a 1.5-m organic black fine sand containing root fragments and a total organic matter content of 36% with a hydraulic conductivity of 8.2 m day^{-1}; (C) a transitional 0.3-m gray medium to fine sand with 7% organic matter and a hydraulic conductivity of 16.9 m day^{-1}; and layer (D) identified as a clear gray medium sand from 2.3- to 3-m depth with a hydraulic conductivity of 22.1 m day^{-1} (Figs. S4b and 6b). Based on the hydrogeological studies developed in Chandler et al. (1985) and Ellis (2013), layer D probably corresponds to Aquifer A2 in the Miocene-Pliocene Aquifer. Based on the ERT measurements and sediment cores collected 100 m off the shore at TS-NE in July 2018, this sequence of sediment layers is also present in the northeastern shore. However, the sediment core collected on the shore of site TS-NE was 3.5-m long and showed no vertical structure (Fig. S4c); the entire core consisted of coarse sand (E), typical for anthropogenically developed beach areas. The hydraulic conductivity of this layer was the highest of all sediment layers identified during this study with 58.4 m day^{-1} (Fig. 6c).

Quantification of SGD

SGD Variability

To evaluate the driving forces that control SGD and observe its temporal variability in Mobile Bay, we measured the hourly SGD rates continuously during 5 days at all three study sites

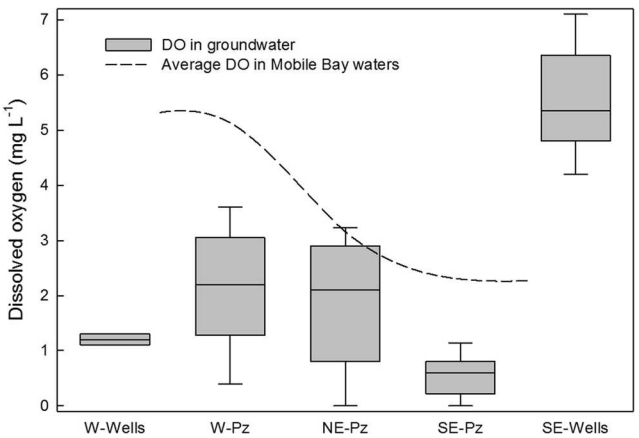

Fig. 5 Box plot showing DO concentrations in groundwater collected from all intertidal piezometers (W-Pz, NE-Pz, and SE-Pz) at all three study sites (TS-W, TS-NE, and TS-SE), from inland wells of the west shore (W-Well), and inland wells of the east shore (SE-Wells). The dashed line represents the average DO concentration measured in surface bay waters along the western, northeastern, and southeastern shores of Mobile Bay

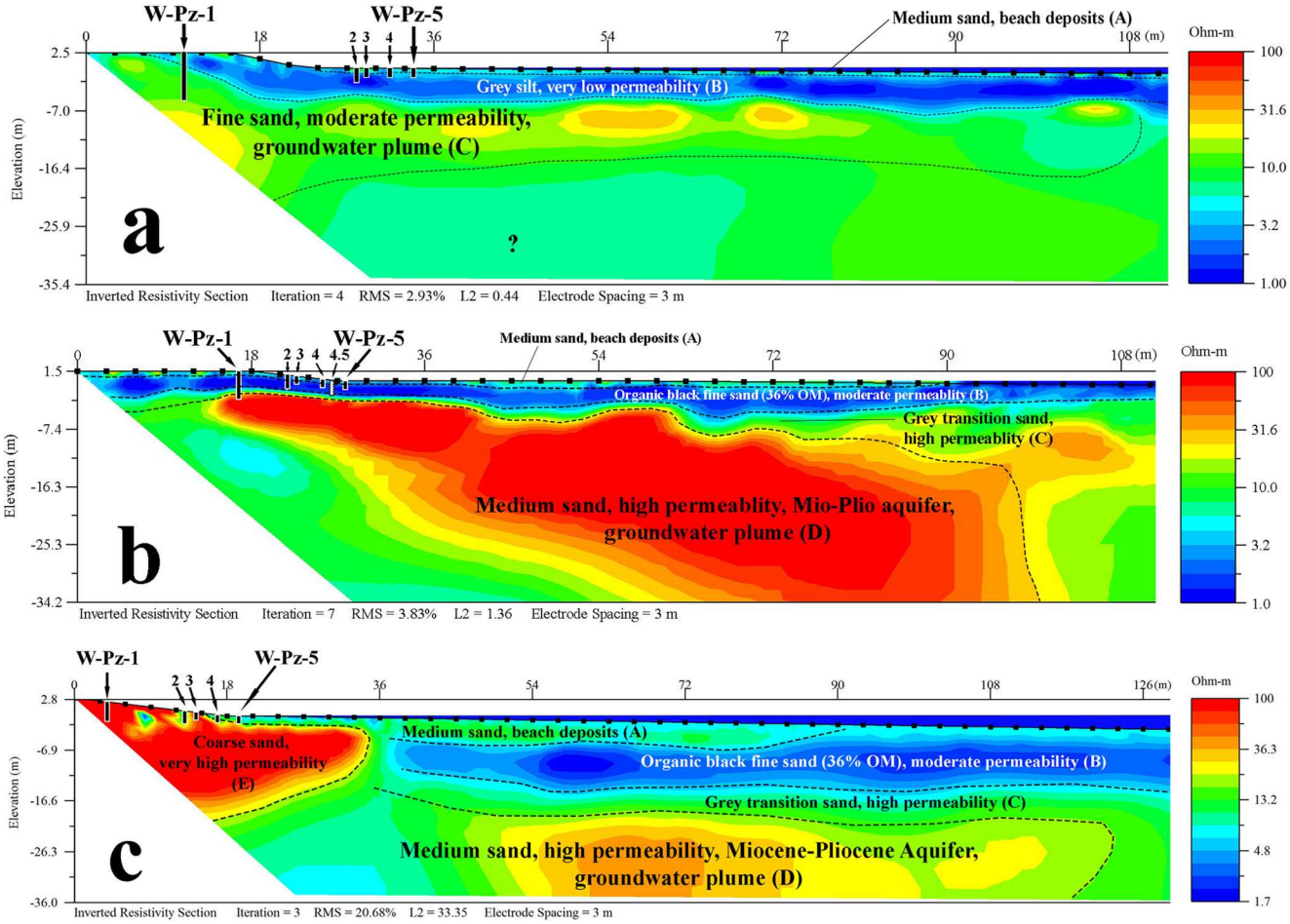

Fig. 6 Shore-perpendicular electrical resistivity tomography (ERT) image and geologic interpretation at study site TS-W on the western shore (**a**), study site TS-SE on the southeastern shore (**b**), and study site TS-NE on the northeastern shore (**c**). The location and depth of piezometers (Pz-1 to Pz-5) are also shown on each panel. On the western shore, we identified a 2.5-m thick silt layer at TS-W and a groundwater plume extent of 80 m (**a**); at study site TS-SE a 1.5-m thick organic fine sand layer with up to 36% organic matter was found above the medium sand Miocene-Pliocene Aquifer with a groundwater plume extent of 70 m (**b**); whereas at study site TS-NE, we found that an artificially added coarse sand deposit was present at the beach area as well as the fine sand organic layer and the underlying Miocene-Pliocene Aquifer with a groundwater plume extent of 100 m (**c**). Dashed lines at each ERT image depict the interphase between sediment layers

during March 13–18 of 2016. During these SGD time-series measurements, we captured the response of the system to two torrential rain events between March 11 and March 18. In March 11, the area received ~ 100 mm of rain (rain event 1) and in March 17–18, a second rain event of 80 mm (rain event 2) took place. Groundwater elevation data from well GSA-B3 (obtained from http://www2.gsa.state.al.us/gsa/water/realtime_monitoring.html) and well USGS-WB (obtained from https://groundwaterwatch.usgs.gov/) showed that each rain event was followed by a gradual increase in the Miocene-Pliocene Aquifer elevation in all study sites (Fig. 7).

On the western shore, the tidal stage and the SGD rates showed a negative correlation ($R^2 = 0.75$) during the entire time-series (Fig. 7a, Figs. S5a and S5b). The SGD rates were positively correlated with the groundwater elevation of the Miocene-Pliocene Aquifer ($R^2 = 0.21$) during the entire time-series (Figs. 7a and S5c). On the northeastern shore, the tidal stage and the SGD rates were negatively correlated only during the first day of measurements ($R^2 = 0.77$) (Figs. 7b and S6a). After the second day, we found that the SGD rates were positively correlated with the groundwater elevation of the Miocene-Pliocene Aquifer ($R^2 = 0.68$) (Figs. 7 and S6b). On the southeastern shore, the tidal stage was also negatively correlated with SGD throughout the measurement period ($R^2 = 0.38$) (Figs. 7c and S7a) with the maximum correlation found after the second day of measurements ($R^2 = 0.69$) (Figs. 7c and S7b). A positive correlation between SGD and the groundwater elevation was found during the 5-day time-series ($R^2 = 0.17$) where SGD experienced a general decline as the groundwater elevation decreased (Figs. 7c and S7c).

Table 1 Sediment properties of the three cores extracted at each study site (TS-W, TS-SE, and TS-NE) including grain size, density, porosity, organic matter content, and hydraulic conductivity of all sediment layers identified. At study site TS-W, the silt layer (B) restricted groundwater flow from layer C in which we observed a SGD plume extending 80 m in the ERT images; at study site TS-SE, we observed that SGD occurred from layer D through the organic layer (B) extending 70 m; whereas at study site TS-NE SGD occurred preferentially through the coarse sand (A) and through the organic layer (B) with a SGD plume extending 100 m in layer D

Core ID	Layer (From top to bottom)	Predominant grain size	Grain density (g cm^{-3})	Porosity	Organic matter content (%)	Hydraulic conductivity (m day^{-1})
TS-W	A	Medium sand (70%)	1.44	0.32	2	10.5
	B	Coarse silt (68%)	2.39	0.50	12	4.1
	C	Fine sand (58%)	1.68	0.42	5	7.9
TS-SE	A	Medium sand (75%)	1.54	0.27	3	11.5
	B	Fine sand (80%)	1.30	0.46	36	8.2
	C	Medium sand (65%)	1.28	0.38	7	16.9
	D	Medium sand (78%)	1.19	0.23	2	22.1
TS-NE	E	Coarse sand (75%)	2.24	0.36	1	58.4
	A	Medium sand (75%)	1.54	0.27	3	11.5
	B	Fine sand (80%)	1.30	0.46	36	8.2
	C	Medium sand (65%)	1.28	0.38	7	16.9
	D	Medium sand (78%)	1.19	0.23	2	22.1

Total SGD Assessments

Using the ^{222}Rn mass balance, we calculated that the groundwater specific discharge (ω) on the western shore (study site TS-W) during dry seasons was on average 5 ± 1 cm day^{-1} ($n = 2$), while during dry seasons, the specific discharge averaged 6 ± 2 cm day^{-1} ($n = 2$) (Table 2). Using seepage meter deployments at this site during the dry season, we found an average specific discharge of 4 ± 1 cm day^{-1} ($n = 24$). To obtain groundwater fluxes (SGD) applying Eq. S3, a seepage area (A) of 3.8×10^6 m^2 was calculated by multiplying the SGD plume extent of 80 m based on shore-perpendicular ERT measurements during low tide (Fig. 6a) and a coastline length of 47.6×10^3 m, determined by radon anomalies during boat surveys (Fig. 2a). Combining results from the ^{222}Rn mass balance and seepage meter measurements, we calculated a total SGD flux to the western shore of Mobile Bay of $1.8 \pm 0.6 \times 10^5$ m^3 day^{-1} ($n = 2$) during the dry seasons and $2.4 \pm 0.7 \times 10^5$ m^3 day^{-1} ($n = 2$) during the wet seasons (Table 2, Fig. 8). All terms of the ^{222}Rn mass balance during each sampling campaign are shown in Table 2.

On the southeastern shore of Mobile Bay at study site TS-SE, the average groundwater specific discharge (ω) was 17 ± 5 cm day^{-1} ($n = 3$) during dry seasons and 23 ± 7 cm day^{-1} ($n = 3$) during wet seasons. The average specific discharge determined from the two seepage meter deployments during a dry season was 9 ± 3 cm day^{-1} ($n = 24$). Using shore-perpendicular ERT measurements and radon surveys at the SE study site, a seepage area (A) of 1.5×10^6 m^2 was calculated using the groundwater plume extent of 70 m (Fig. 6b) and a coastline length of 21.5×10^3 m. Combined total SGD from the ^{222}Rn mass balance and seepage meters at TS-SE ranged between $2.3 \pm 1.0 \times 10^5$ m^3 day^{-1} ($n = 3$) during three dry seasons and $3.8 \pm 1.3 \times 10^5$ m^3 day^{-1} ($n = 3$) during three wet seasons (Table 2, Fig. 8).

At study site TS-NE on the northeastern shore of Mobile Bay, the average specific discharge (ω) was 16 ± 6 cm day^{-1} ($n = 2$) during dry seasons and 24 ± 9 cm day^{-1} ($n = 2$) during wet seasons. Average specific discharge was 17 ± 4 cm day^{-1} ($n = 24$) using seepage meter measurements during a dry season. The groundwater plume extent (from ERT shore-perpendicular measurements) of 100 m (Fig. 6c) and a coastline length of 2.3×10^3 m (from ^{222}Rn anomalies surveys) were used to calculate a seepage area (A) of 2.3×10^5 m^2. Average SGD derived from the ^{222}Rn mass balance and seepage meters during two dry and wet seasons was $3.9 \pm 1.7 \times 10^5$ ($n = 2$) and $5.7 \pm 2.1 \times 10^5$ m^3 day^{-1} ($n = 2$), respectively (Table 2, Fig. 8).

Combining the groundwater fluxes measured at all three study sites (TS-W, TS-SE, and TS-NE), we found that the total SGD (combined FSGD and RSGD) to Mobile Bay using the ^{222}Rn and seepage meter methods ranged between $8.0 \pm 3.3 \times 10^5$ m^3 day^{-1} during dry seasons and $11.9 \pm 4.1 \times 10^5$ m^3 day^{-1} during wet seasons (Table 2, Fig. 8).

FSGD and RSGD Individual Assessments

Using the radium isotopes mixing model (Eqs. S5, S6, and S7), we calculated that the average brackish recirculated SGD (RSGD) on the western shore at study site TS-W ranged between $0.7 \pm 0.2 \times 10^5$ m^3 day^{-1} ($n = 2$) during dry seasons and $1.6 \pm 0.4 \times 10^5$ m^3 day^{-1} ($n = 2$) during wet seasons (Table 3).

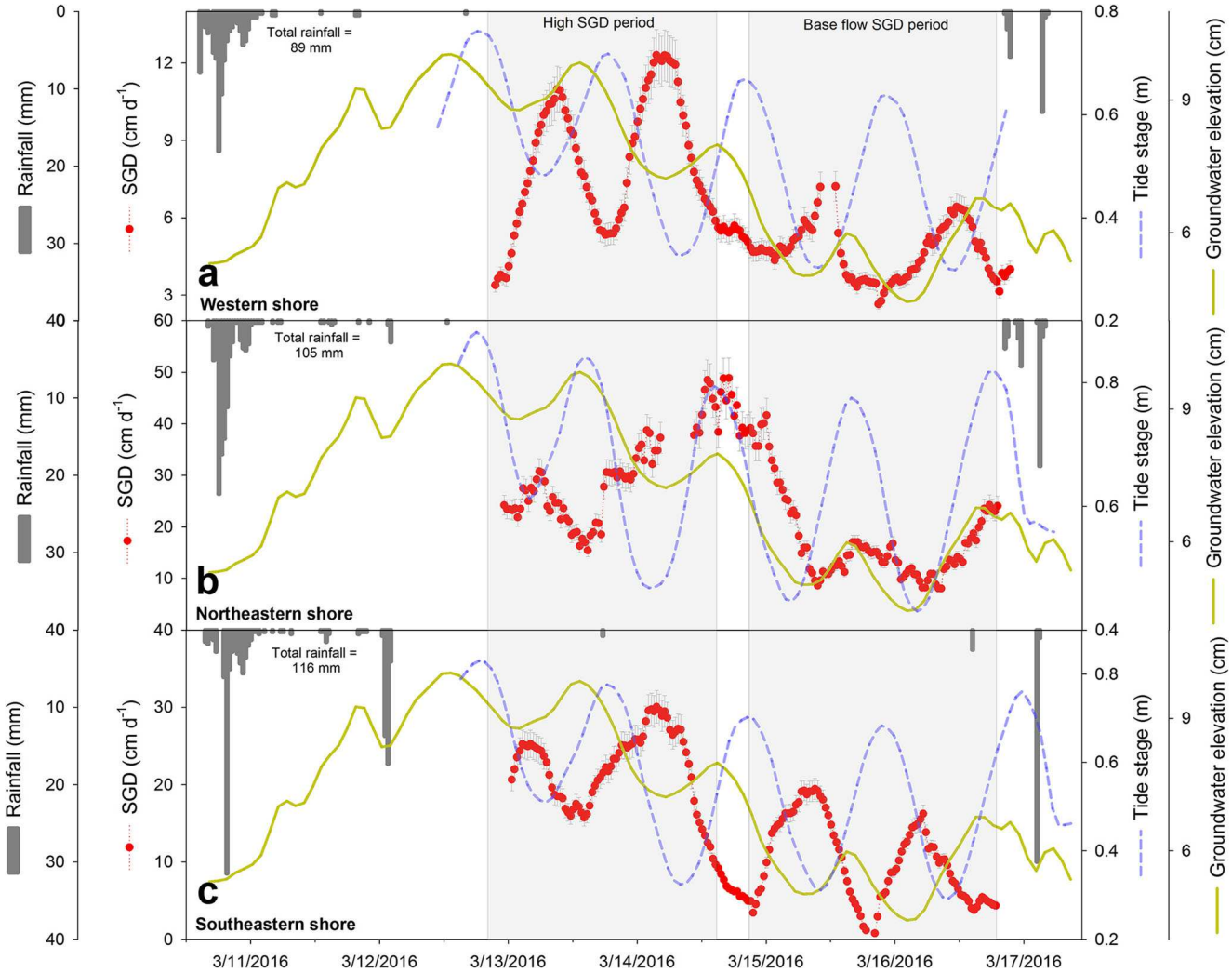

Fig. 7 Temporal variation of SGD rates (cm day^{-1}) with respect to tide stage (m) in Mobile Bay, precipitation (mm), and groundwater elevation (cm) of the Miocene-Pliocene Aquifer during March 13–18 at study site TS-W on the western shore (**a**), TS-NE on the northeastern shore (**b**), and TS-SE on the southeastern shore (**c**). Two rain events occurred prior (March 11–12) and after (March 17–18) the time-series measurements, which were followed by a peak in the groundwater elevation after less than 2 days. Maximum SGD rates were reached after 3–4 days in all study sites

On the southeastern shore at study site TS-SE, RSGD was $1.1 \pm 0.3 \times 10^5$ m^3 day^{-1} ($n = 3$) during dry seasons and $1.7 \pm 0.4 \times 10^5$ m^3 day^{-1} ($n = 3$) during wet seasons, whereas on the northeastern shore at study site TS-NE, RSGD was $1.5 \pm 0.3 \times 10^5$ m^3 day^{-1} ($n = 2$) during dry and $3.2 \pm 0.6 \times 10^5$ m^3 day^{-1} ($n = 2$) during wet seasons (Table 3). All terms used in the radium mixing model are shown in Table 3.

To calculate FSGD and RSGD independently of the radioisotope approaches, we also applied two site- and season-specific end-member mixing models using $\delta^{18}O$ and $\delta^{2}H$ (Eqs. S9 and S10). Using this approach, we found that on the western shore (TS-W) RSGD represented 56% of the total SGD during dry seasons and 30% during wet seasons (Table 4). In comparison, based on the radium method, RSGD represented 38% and 66% during the dry and wet seasons (Table 3). On the southeastern shore (TS-SE), RSGD accounted for 43 (dry) to 31% (wet) and 48 (dry) to 45% (wet) using the radium approach. On the northeastern shore (TS-NE), RSGD ranged from 30 (dry) to 27% (wet), whereas the radium method yielded contributions of 38 (dry) to 56% (wet) (Tables 3 and 4).

Based on these proportions and considering the total SGD obtained from the ^{222}Rn and seepage meter methods, FSGD in the western shore at study site TS-W was between $0.8 \pm 0.3 \times 10^5$ m^3 day^{-1} during dry season and $1.7 \pm 0.5 \times 10^5$ m^3 day^{-1} during the wet seasons. On the southeastern shore at study site TS-SE, FSGD ranged between $1.2 \pm 0.4 \times 10^5$ and $2.6 \pm 0.9 \times 10^5$ m^3 day^{-1}; whereas at the northeastern shore study site TS-NE, FSGD was $2.7 \pm 1.1 \times 10^5$ to $4.2 \pm 1.6 \times 10^5$ m^3 day^{-1} (Table 4, Fig. 8). Combining the FSGD from all sections,

Table 2 Radon mass balance to assess the total SGD at each study site (TS-W, TS-SE, and TS-NE) during all sampling campaigns. Seepage velocity (ω) and groundwater fluxes (SGD) obtained from seepage meters deployments during June 2016 are also shown for each study site. The average groundwater fluxes (SGD) during the dry and wet seasons are shown for each site. Additionally, the total SGD in Mobile Bay from all study sites is presented as a range including uncertainties during each sampling campaign

Location	Season	Sampling campaign	F_{Atm} ($\times 10^3$ dpm m^{-2} day^{-1})	F_{Mix}	F_{Diff}	C_{Ra} (dpm m^{-3})	Rn_{SGD} ($\times 10^3$ dpm m^{-3})	A ($\times 10^6$ m^2)	ω (cm day^{-1})	SGD ($\times 10^5$ m^3 day^{-1})
TS-W	Dry	July-15	3 ± 1	10 ± 3	0.3 ± 0.02	620 ± 60	230 ± 30	3.8	6 ± 2	2.2 ± 0.6
		June-16	6 ± 2	11 ± 4	0.5 ± 0.04	450 ± 50	230 ± 30	3.8	4 ± 1	1.3 ± 0.4
		June-16	Seepage meter measurements					3.8	6 ± 1	2.0 ± 0.3
									Average	1.8 ± 0.6
	Wet	March-15	8 ± 3	43 ± 12	0.5 ± 0.03	130 ± 10	230 ± 30	3.8	6 ± 2	2.4 ± 0.7
		March-16	17 ± 5	6 ± 2	0.4 ± 0.04	250 ± 20	230 ± 30	3.8	6 ± 2	2.4 ± 0.7
									Average	2.4 ± 0.7
TS-SE	Dry	July-15	6 ± 3	21 ± 8	0.6 ± 0.07	240 ± 20	50 ± 10	1.5	20 ± 6	3.0 ± 0.9
		March-17	0.1 ± 0.01	19 ± 7	0.4 ± 0.05	190 ± 10	50 ± 10	1.5	20 ± 6	3.0 ± 1.0
		June-16	3 ± 1	9 ± 3	0.5 ± 0.06	40 ± 3	50 ± 10	1.5	13 ± 4	2.0 ± 1.0
		June-16	Seepage meter measurements					1.5	9 ± 3	1.4 ± 0.7
									Average	2.3 ± 1.0
	Wet	March-15	8 ± 3	57 ± 14	0.3 ± 0.03	90 ± 5	50 ± 10	1.5	28 ± 9	4.2 ± 1.3
		March-16	32 ± 12	3 ± 1	0.4 ± 0.04	230 ± 10	50 ± 10	1.5	22 ± 7	3.3 ± 1.1
		July-17	2 ± 0.4	35 ± 10	0.5 ± 0.07	290 ± 20	50 ± 10	1.5	25 ± 8	3.8 ± 0.3
									Average	3.8 ± 1.3
TS-NE	Dry	June-16	2 ± 0.08	17 ± 6	0.4 ± 0.03	170 ± 20	60 ± 20	2.3	14 ± 5	3.2 ± 1.1
		June-16	Seepage meter measurements					2.3	17 ± 4	3.9 ± 0.9
		March-17	0.5 ± 0.1	28 ± 9	0.4 ± 0.05	190 ± 10	60 ± 20	2.3	20 ± 7	4.6 ± 1.7
									Average	3.9 ± 1.7
	Wet	March-16	14 ± 4	8 ± 2	0.3 ± 0.03	190 ± 20	60 ± 20	2.3	24 ± 9	5.7 ± 2.0
		July-17	9 ± 2	56 ± 19	0.5 ± 0.07	80 ± 6	60 ± 20	2.3	25 ± 9	5.8 ± 2.1
									Average	5.7 ± 2.1
Mobile Bay									Dry	4.7–11.3
								Total		
									Wet	7.8–16.0

the total FSGD to Mobile Bay ranged between 2.8×10^5 m^3 day^{-1} during the dry season and 11.5×10^5 m^3 day^{-1} during the rainy season, considering all uncertainties (Table 4).

Discussion

Hydrodynamics in Mobile Bay

We found that the residence time in Mobile Bay varied seasonally and was primarily controlled by the Mobile-Tensaw River System discharge. The average water apparent age in Mobile Bay during the wet season was 5.1 days when the river flux was on average 2450×10^5 m^3 day^{-1}, whereas during dry seasons, it was 7.0 days when the river discharge was on average 260×10^5 m^3 day^{-1}. These values are comparable to other river-dominated estuaries with similar river fluxes and basin morphologies (e.g., Dulaiova et al. 2006). For instance, Dulaiova and Burnett (2008) determined that the residence time in the Apalachicola Bay (FL), a similar estuary in the Northern Gulf of Mexico, was governed by the magnitude of the Apalachicola River discharge. During high flow conditions (878×10^5 m^3 day^{-1}) Dulaiova and Burnett (2008) using a similar approach estimated an average residence time of 6.9 days compared to 13.0 days during low discharge (292×10^5 m^3 day^{-1}).

Based on the spatial distribution of the water apparent ages determined by this study, we found that during high flow conditions, the water circulation of the river plume in Mobile Bay occurs counterclockwise. Younger ages (1.0–2.4 days) were found at the mouth of the river (as to be expected) and along the western shore of the bay (2.5–4.9 days). In contrast, older ages were detected near Main Pass (5.4–6.0 days), along the east shore of Mobile Bay (3.8–7.8 days), and Bon Secour Bay (7.8–10.3 days) (Fig. 3b). These longer

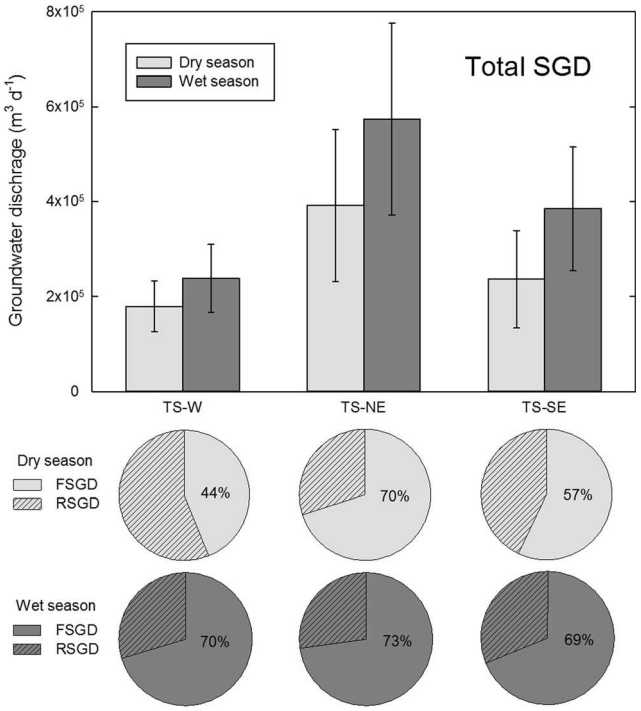

Fig. 8 The upper bar plot shows the total SGD in Mobile Bay (m^3 day^{-1}) showing groundwater discharge measured at all three study sites (TS-W, TS-NE, and TS-SE) during the dry (light gray) and wet (dark gray) seasons. The lower panel shows a comparison between the fresh SGD (FSGD) and recirculated SGD (RSGD) components of the total SGD during dry and wet seasons

residence times measured along the southeastern area of the bay are the result of the Mobile Bay's geometry and local winds (Noble et al. 1996; Park et al. 2007; Dzwonkowski et al. 2011). We suggest that Dauphin Island and the Fort Morgan Peninsula deflect part of the estuary's outflow, which is then most likely forced towards the east by the prevailing easterly winds that were present during all sampling campaigns (https://tidesandcurrents.noaa.gov). This spatial distribution is in excellent agreement with estimations reported in Webb and Marr (2016) using a numerical modeling approach to determine the bay circulation. The model yielded lower residence time values (1–6 days) for the western shore and mid-bay area and higher residence times (8 and 14 days) on the southeastern shore and Bon Secour Bay. Furthermore, salinity distributions in Mobile Bay during our 3-year study during high flow conditions confirmed this circulation pattern as well (Fig. S2b). Low salinities (0.1–2.0) attributed to the freshwater plume of the Mobile-Tensaw River System were observed to extend from the river delta towards Main Pass along the mid-bay area (Fig. S2b). Consistently with the water ages, the highest salinity values within the Bay were measured in Bon Secour Bay (4.5–6.0), also indicating that the water tends to remain stagnant in this area, where evaporation leads to higher salinity values (Fig. S2b).

However, we also observed that during the dry season (i.e., low flow conditions), the described circulation pattern was not that apparent. The water residence time increased equally along the east (2.3–14.9) and west (2.6–11.9 days) shores; with a gradual increase across the bay from the river delta to the south (Fig. 3a). We observed relatively long residence times in the mid-bay area (2.9–8.0 days), indicating that the river plume moved preferentially near the shores (Fig. 3a). The salinity distribution measured during the dry season also supports this pattern, with relatively higher values in the mid-bay area (6.0–10.0) and gradual increase along the eastern (1.0–12.0) and western shores (1.5–17.0) (Fig. S2a). These findings based on radiotracer field data were also confirmed by Du et al. (2018), who also found that during the wet season the river plume flows preferentially along the western shore and mid-bay area of Mobile Bay, whereas Bon Secour Bay and the southeastern shore remain unaffected by the flushing effect of the river discharge. During the dry season, Du et al. (2018) also observed that the flow direction diverts towards the west and east shores from the river delta towards Main Pass. Furthermore, using a modeling approach, Du et al. (2018) found significantly higher residence times in Bon Secour Bay and the southeastern section during both wet and dry seasons (12–48 days), also indicating the water tendency to remain stagnant in this area.

Based on these bay water circulation patterns and using the water residence times estimated in this study, we also calculated the average water flushing rate (km day^{-1}) in Mobile Bay, Alabama. Flushing rate is an extremely important parameter for estuarine ecosystems. Most often the flushing rates are applied to study the transport dynamics of dissolved contaminants and suspended particles in the bay. Specifically for Mobile Bay, understanding the transport timescales of terrestrial material in the estuary and their export to the Gulf of Mexico is essential to further study the impact on the estuarine and marine ecosystems on the Gulf system (Moore and Krest 2004; Peterson et al. 2008). As in other similar studies (e.g., Moore 2000; Dulaiova et al. 2006), we define this term as the time that the river water inputs take to flow across the 46-km transect from the river delta to Main Pass, considering the water circulation described above. Based on the apparent water ages and following the methodology described by Moore (2000), we estimated that the flushing rate in Mobile Bay ranged from 3.3 km day^{-1} during the dry season (when the river flux was 260×10^5 m^3 day^{-1}) to 4.7 km day^{-1} during the wet season (when the river flux was 2450×10^5 m^3 day^{-1}). These flushing rate variations in Mobile Bay during contrasting river discharge indicate a dependence on river flow conditions.

Table 3 Summary of values for all parameters used in the radium mixing models to assess the recirculated SGD (RSGD) at each study site (TS-W, TS-SE, and TS-NE) during the dry and wet seasons. The fraction of RSGD (f_{RSGD}) with respect to the total inputs (RSGD, river, and the seawater from the Gulf of Mexico) obtained when solving the models is shown along with the respective RSGD. The total RSGD in Mobile Bay is presented as a range including uncertainties during each sampling campaign

Location	Season	Sampling campaign	$^{226}Ra_{River}$ (dpm m^{-3})	$^{224}Ra_{River}$	$^{226}Ra_{RSGD}$	$^{224}Ra_{RSGD}$	$^{226}Ra_{ow}$	$^{224}Ra_{ow}$	$^{226}Ra_{MB}$	$^{224}Ra_{MB}$	t (day)	V ($\times 10^6$ m^3)	f_{RSGD} (%)	RSGD ($\times 10^5$ m^3 day^{-1})
TS-W	Dry	July-15	20 ± 2	10 ± 2	6610 ± 500	1130 ± 100	90 ± 5	20 ± 3	620 ± 30	200 ± 10	6 ± 0.3	7.6	8	1.0 ± 0.2
		June-16	200 ± 20	70 ± 2	6610 ± 500	1130 ± 100	20 ± 2	10 ± 1	50 ± 4	100 ± 7	4 ± 0.2	7.6	3	0.5 ± 0.1
												Average		0.7 ± 0.2
	Wet	March-15	100 ± 7	40 ± 3	6610 ± 500	1130 ± 100	40 ± 3	40 ± 4	90 ± 5	70 ± 3	6 ± 0.4	7.6	17	2.1 ± 0.4
		March-16	100 ± 7	40 ± 3	6610 ± 500	1130 ± 100	40 ± 3	40 ± 4	250 ± 20	90 ± 8	7 ± 0.5	7.6	10	1.1 ± 0.2
	Average											Average		1.6 ± 0.4
TS-SE	Dry	July-15	20 ± 2	10 ± 2	350 ± 20	340 ± 20	90 ± 5	20 ± 3	240 ± 20	100 ± 10	7 ± 0.6	3.0	23	1.0 ± 0.2
		March-17	180 ± 10	80 ± 7	350 ± 20	340 ± 20	20 ± 2	10 ± 1	230 ± 10	220 ± 20	8 ± 0.6	3.0	35	1.3 ± 0.3
		June-16	200 ± 20	70 ± 2	350 ± 20	340 ± 20	20 ± 2	10 ± 1	50 ± 4	60 ± 5	6 ± 0.4	3.0	18	0.9 ± 0.2
	Average											Average		1.1 ± 0.3
	Wet	March-15	100 ± 7	40 ± 3	700 ± 40	470 ± 30	40 ± 3	40 ± 4	90 ± 5	90 ± 5	4 ± 0.3	3.0	18	1.4 ± 0.3
		March-16	100 ± 7	40 ± 3	700 ± 40	470 ± 30	40 ± 3	40 ± 4	230 ± 10	220 ± 20	9 ± 0.7	3.0	57	1.9 ± 0.4
		July-17	180 ± 10	80 ± 7	700 ± 40	470 ± 30	70 ± 5	50 ± 3	170 ± 10	80 ± 7	5 ± 0.4	3.0	29	1.7 ± 0.4
	Average											Average		1.7 ± 0.4
TS-NE	Dry	June-16	200 ± 20	70 ± 2	540 ± 40	480 ± 30	20 ± 2	10 ± 1	170 ± 10	140 ± 10	7 ± 0.6	4.7	24	1.6 ± 0.3
		March-17	180 ± 10	80 ± 7	540 ± 40	480 ± 30	20 ± 2	10 ± 1	60 ± 4	70 ± 5	8 ± 0.6	4.7	30	1.4 ± 0.3
	Average											Average		1.5 ± 0.3
	Wet	March-16	100 ± 7	40 ± 3	600 ± 40	430 ± 30	40 ± 3	40 ± 4	190 ± 20	130 ± 10	10 ± 0.9	4.7	68	3.2 ± 0.6
		July-17	180 ± 10	80 ± 7	600 ± 40	430 ± 30	70 ± 5	50 ± 3	80 ± 6	130 ± 10	4 ± 0.3	4.7	25	3.3 ± 0.6
	Average											Average		3.2 ± 0.6
Mobile Bay												Dry		2.5–4.1
												Total		
												Wet		5.1–8.9

Table 4 End-member values used in the site- and season-specific $\delta^{18}O$ and $\delta^{2}H$ mixing models utilized to calculate the proportional fraction of fresh SGD (FSGD) and recirculated SGD (RSGD) from the total SGD at all three study sites (TS-W, TS-SE, and TS-NE) during the dry and wet seasons. The fraction of both FSGD and RSGD (f_{FSGD} and f_{RSGD}) are also shown for each mixing model and their average (average f_{FSGD} and f_{RSGD}) for each study site during the dry and wet seasons. The FSGD and RSGD values shown in the table were obtained by multiplying the average f_{FSGD} and average f_{RSGD} components by the average total SGD (SGD) presented in Table 3, measured during each season at each of the three study sites. The total FSGD and RSGD in Mobile Bay are presented as a range including variations during each sampling campaign

Location	Season	$\delta^{18}O_{FSGD}$ (‰ VSMOW)	$\delta^{18}O_{RSGD}$	$\delta^{18}O_{SGD}$	f_{FSGD} (%)	f_{RSGD}	$\delta^{2}H_{FSGD}$ (‰ VSMOW)	$\delta^{2}H_{RSGD}$	$\delta^{2}H_{SGD}$	f_{FSGD} (%)	f_{RSGD}	Average f_{FSGD} (%)	Average f_{RSGD}	FSGD ($\times 10^5$ m^3 day^{-1})	RSGD
TS-W	Dry	−4.2	−0.5	−2.1	45	55	−20	0	−9	43	57	44 ± 6	56 ± 7	0.8 ± 0.3	1.0 ± 0.3
	Wet	−4.2	−1.5	−3.4	71	29	−20	−7	−16	70	30	70 ± 8	30 ± 3	1.7 ± 0.5	0.7 ± 0.2
TS-SE	Dry	−4.0	−0.2	−2.5	60	40	−20	0	−11	54	46	57 ± 10	43 ± 8	1.2 ± 0.4	1.0 ± 0.3
	Wet	−4.2	−2.8	−3.8	70	30	−20	−10	−17	68	32	69 ± 5	31 ± 2	2.6 ± 0.9	1.2 ± 0.4
TS-NE	Dry	−4.0	−2.2	−3.6	74	26	−20	−10	−17	67	33	70 ± 8	30 ± 4	2.7 ± 1.1	1.2 ± 0.4
	Wet	−4.2	−3.9	−4.1	66	34	−20	−18	−20	80	20	73 ± 3	27 ± 1	4.2 ± 1.6	1.5 ± 0.5
Mobile Bay	Dry												Total	2.8–6.5	2.2–4.2
	Wet													5.5–11.5	2.3–4.5

SGD Dynamics and Driving Forces

We found that the magnitude and dynamics of SGD in Mobile Bay (Alabama) were controlled mainly by two driving forces including (i) terrestrial hydraulic gradients in the coastal aquifer and (ii) tidal pumping (Moore 2010; Santos et al. 2012). On a large (annual) time-scale, the dominant mechanism controlling SGD was the terrestrially driven variations in the hydraulic gradient of Miocene-Pliocene Aquifer across the watershed. We found that at an annual scale tidal forcing did not affect the SGD dynamics significantly, which instead, followed the groundwater elevation fluctuations (Fig. 9). Changes in the terrestrial hydraulic gradient were responsible for the seasonal variations of SGD rates observed throughout the Mobile Bay coastline (Fig. 8). During the wet season, we observed that high precipitation rates increased the Miocene-Pliocene Aquifer groundwater table creating higher hydraulic gradients near the coastlines of Mobile Bay and resulting in enhanced SGD a few days later (Fig. 9). We found that SGD was on average 35% higher during the wet season (11.9×10^5 m^3 day^{-1}) throughout the Mobile Bay coastal zone compared to the dry season (8.0×10^5 m^3 day^{-1}) (Table 2, Fig. 9). However, we found that the magnitude of these longer-term terrestrially driven seasonal variations of SGD were also site-specific. For instance, the highest (up to 40%) SGD difference between seasons was measured on the southeastern shore compared to the 32% difference on the northeastern shore and 25% on the western shore (Table 2).

On a short (daily) time-scale, SGD at each of our study sites in Mobile Bay (TS-W, TS-NE, TS-SE) was modulated by a combination of marine (tidal pumping) and terrestrial (hydraulic gradient) forces, with marine forcing prevailing during base flow conditions. An illustration of this site-specific behavior was evident throughout the continuous five-day record conducted at each of the study sites (TS-W, TS-SE, and TS-NE) during one of the rainy seasons (Fig. 7). A heavy rain event (average 100 mm) 2 days prior to our deployment resulted in a gradual increase of the Miocene-Pliocene Aquifer level throughout the research area. The maximum groundwater elevation after the storm event coincided with the beginning of our deployments. As the local water table was gradually decreasing during the first 2 days of our deployment, we observed a significant decrease in the SGD rates of approximately 45% at all three sites (Fig. 7a, b, c). We found that on average, it took about 2–3 days for the water table to gradually return to base flow conditions. This 5-day record that included the high water table and base flow conditions provided us with the rare opportunity to examine the hydraulic response at each of the study sites. During this continuous record, we distinguished two periods that corresponded to high and low SGD fluxes and we

refer hereafter as "high SGD period" and "base flow SGD period" (Fig. 7).

We found that on the western shore of Mobile Bay at study site TS-W (Fig. 1), SGD was mainly controlled by tidal pumping (Santos et al. 2012) both during the high and base/low flow conditions (Fig. 7a). An evidence for this discharge mechanism is strongly supported by a good correlation (R^2 = 0.75, Figs. S5a and S5b) between the tide stage, which was used as a proxy for tidal pumping and SGD rates at this location. Indeed, high SGD rates were always observed during low tide whereas lower discharge was found during high tide (Fig. 7a). However, on average, higher discharge rates (9 cm day^{-1}) were detected during the high SGD period (i.e., high water table), and lower SGD (5 cm day^{-1}) was found at the tail of the groundwater elevation decrease (i.e., towards base flow conditions). Nevertheless, the total discharge at this study site was always much lower compared to the other two study sites on the east shore (Fig. 8). Tidal pumping was also confirmed at the western shore of Mobile Bay by the time-lapsed ERT measurements conducted during one of the dry seasons (July 2015) of this study. Although the tidal prism at this site is the smallest, during the shore-perpendicular ERT deployment at TS-W, we observed an overall 18% increase in the size of the SGD plume during falling tide (Fig. S4a). Finally, we also found that these characteristics also promoted the highest seawater recirculation (RSGD) of the three sites in Mobile Bay and the maximum contrast between wet and dry seasons (30–56%) (Fig. 8).

On the northeastern shore at study site TS-NE, the terrestrially driven hydraulic gradient was the primary SGD driver during this continuous record. The correlation between the hydraulic head and SGD was significant ($R^2 = 0.68$, Fig. S6b) throughout the 4 days of deployment. However, tidal pumping was also an evident driving mechanism for SGD during base flow conditions (Figs. 7b and S6a). This was confirmed by the time-lapsed ERT measurements conducted during the dry season (Fig. S4c). Using these ERT images, we found that the SGD plume increased about 56% in the transition from high to low tide (Fig. S4c). However, we suggest that terrestrial forcing dominates the SGD dynamics over tidal pumping in the TS-NE study site. This terrestrial control of SGD was also confirmed by the mostly fresh composition of SGD (between 70 and 73%) during both the dry and wet seasons (Fig. 8).

During this continuous record, we found that SGD on the southeastern shore at study site TS-SE was controlled mostly by tidal pumping and affected by the hydraulic gradients to a lower extent. The negative correlation observed between SGD rates and the tide stage ($R^2 = 0.38$) measured throughout the time-series supports this finding (Fig. S7a). A much better correlation was found during the base flow SGD period when we found a correlation of $R^2 = 0.69$, indicating that marine forces indeed dominate the system in the southeastern shore (Fig. S6b). However, the SGD rates gradually decreased following the groundwater elevation peak ($R^2 = 0.17$), highlighting the lower importance of the terrestrially driven hydraulic gradient on the SGD rates (Fig. S7c). The time-lapsed ERT images confirmed that tidal pumping is the main factor controlling the SGD rates during base flow conditions with a SGD plume size change of 44% in the transition from high to low tide stage (Fig. S4b). The synergic control of SGD by marine and terrestrial forces was also supported by the seasonal variation of FSGD from dry seasons (57%) to wet seasons (69%) measured in this area (Fig. 8).

Spatial Distribution of SGD

The regional water table indicates a positive hydraulic gradient towards Mobile Bay along the entire extension of its coastline (except along Bon Secour Bay), indicating that SGD could be ubiquitous (Geological Survey of Alabama 2018) (Fig. 1). However, we found that SGD occurs preferentially along the east shore of Mobile Bay throughout the year, i.e., regardless of the season. This was strongly supported by the results from two independent tracer approaches including radon anomalies in surface waters and electrical resistivity distributions (Fig. 2). CRP surveys revealed the highest bulk (lithology and saturating pore water) resistivity values (40–890 Ohm m) along this side of Mobile Bay suggesting the presence of coarser sediments (sand) saturated with fresh groundwater (Fig. 2b). High resistivity values were also measured in the northern part of the bay near the river delta (30 Ohm m), which were associated with the fresh water input from the Mobile-Tensaw River System. In contrast, the lower resistivity measured along the western shore and Bon Secour Bay (2.8 to 10 Ohm m) indicated limited SGD inputs compared to the southeastern and northeastern shores (Fig. 2b). All ^{222}Rn surveys showed positive concentration anomalies along the east shore of Mobile Bay confirming the CRP indication for the presence of enhanced SGD inputs. A ^{222}Rn positive anomaly ("hot spot") was especially pronounced (0.1–5.0 × 10^3 dpm m^{-3}) on the northeastern shore between the towns of Daphne and Fairhope, which is in the immediate vicinity of our study site TS-NE (Fig. 2b). Negative ^{222}Rn anomalies (− 4.1–0.0 × 10^3 dpm m^{-3}), interpreted as an indication of limited discharge, were found in Bon Secour Bay and the western shore (Fig. 2a). A positive anomaly (0.4–1.5 × 10^3 dpm m^{-3}) located in the northern sector of the western shore was persistently detected during all surveys conducted during this study. We found that this ^{222}Rn "hot spot" coincides with the location of the main ship channel in Mobile Bay, which is dredged to a depth of 15 m (Fig. 1). While we still do not have enough evidence, we speculate that such anthropogenic feature may have perforated the shallow Miocene-Pliocene Aquifer, artificially inducing SGD into the water column. Similar effects are known to exist at other

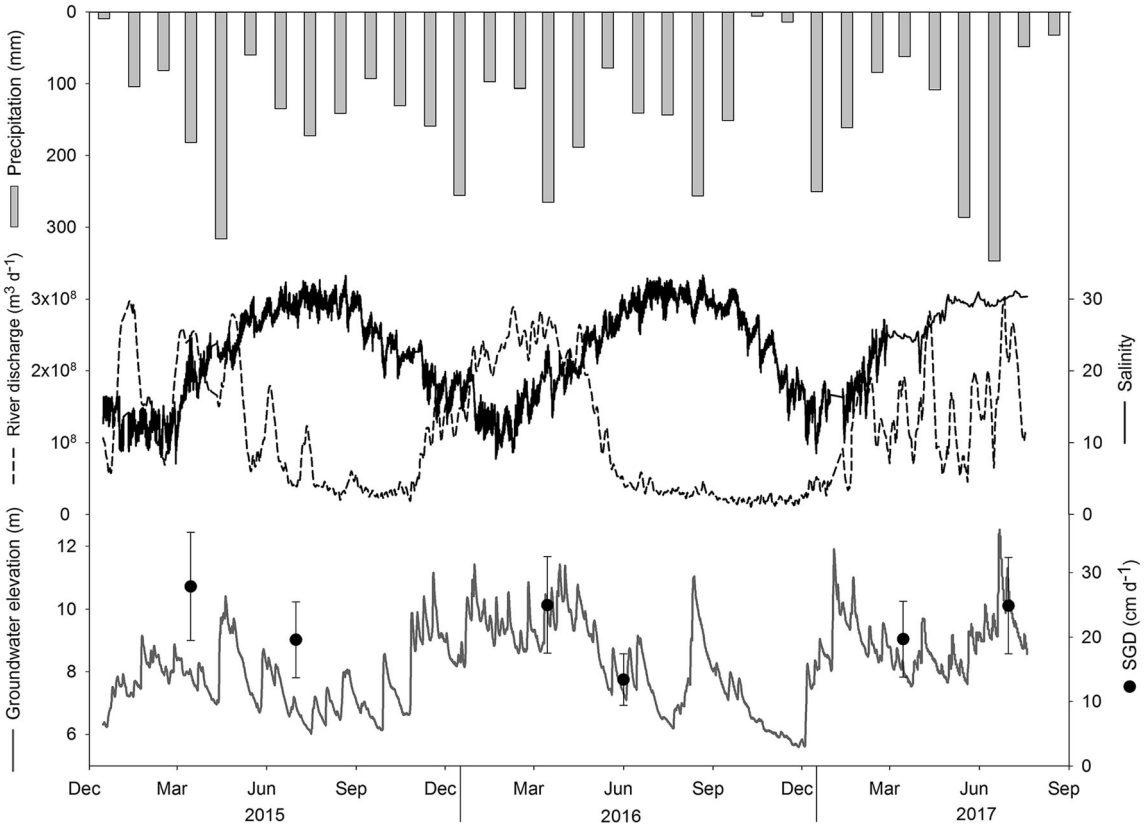

Fig. 9 Three-year time-series of precipitation (mm), Mobile-Tensaw River System discharge (m^3 day^{-1}), salinity in Mobile Bay, groundwater elevation at the Miocene-Pliocene Aquifer (m), and average SGD rates (cm day^{-1}) on the northeastern and southeastern shores (main areas of SGD). Typically, higher rainfall during the wet season (March) coincided with maximum riverine discharge, groundwater elevation, SGD rates, and lowest salinity in Mobile Bay. During 2017 rainfall was lower during March than in June–July, attributed to the occurrence of tropical storm Cindy in Mobile Bay. As a result, we observed the opposite trends: higher river discharge, groundwater elevation, and SGD rates during July compared to March

locations as presented by other studies. For example, Dimova et al. (2013) found that constructed pilings and/or artificial canals in some lakes of Florida have provided new pathways for enhanced groundwater discharge to surface waters.

The described spatial pattern of preferential groundwater discharge to Mobile Bay unveiled by the ^{222}Rn anomalies was also confirmed by the tracer-derived site-specific SGD assessments using multiple isotope approaches (^{222}Rn, ^{224}Ra, and ^{226}Ra) and seepage meters at all three study sites. Throughout the year, during both wet and dry seasons, the calculated SGD rates on the east shore were at least 3 times higher (16–24 cm day^{-1}) than on the western shore (5–6 cm day^{-1}) (Fig. 8, Tables 2 and 3). Although the seepage area (A) of the western shore (3.8×10^6 m^2) was the largest of the three shores, the groundwater fluxes obtained from the radon model and seepage meters deployments were about 40% lower ($1.8–2.4 \times 10^5$ m^3 day^{-1}) compared to the discharge found in the southeastern shore ($2.3–3.8 \times 10^5$ m^3 day^{-1}) and 50% lower compared to the northeastern shore ($3.9–5.7 \times 10^5$ m^3 day^{-1}). Based on our 3-year study, we found that most of the SGD in Mobile Bay occurs on the northeastern shore, accounting for almost 50% of the total SGD to the bay, whereas the southeastern and northeastern shores combined represented ~ 80% of the total (Tables 2 and 3).

We suggest that these results can be explained by the interplay of two main hydrogeological factors: (i) hydraulic gradient variations in the coastal aquifer, mostly result of the regional topographic gradients, and (ii) inherited estuarine lithologic heterogeneities in the coastal shallow sediments that generate preferential groundwater flow paths only in certain areas.

The topographic gradients in the northeastern and southeastern shores are significantly greater than in the western shore, where the land surface is nearly flat 10 km inland away from the shore (Danielson et al. 2013). In contrast, on the northeastern shore the topography gradient near the shore is the largest in Mobile Bay. This topography disposition determines a higher hydraulic gradient of the Miocene-Pliocene Aquifer in Mobile Bay (Fig. 1). The Geological Survey of Alabama (2018) calculated that along the western shore, the hydraulic gradient is 0.07%, along the southeastern shore is

about 0.14%, while the maximum gradient in Mobile Bay is found in the northeastern shore with about 0.25% (Fig. 1). The higher hydraulic gradient of the coastal aquifer is also the primary control for the higher terrestrially driven fresh SGD (FSGD) (Burnett et al. 2003; Santos et al. 2008) observed in the east shore (57–73%) compared to the western shore (44–70%) (Fig. 8). A hydraulic gradient 3.5 and 2 times higher in the southeastern and northeastern shores compared to the western shore can partially explain the higher SGD rates in these two sections.

However, we suggest that the spatial distribution of SGD is additionally controlled to a great extent by inherited estuarine lithologic heterogeneities present in Mobile Bay (Burnett et al. 2006; Holliday et al. 2007). The ERT imaging and sediment cores collected and characterized during this study at the three study sites (TS-W, TS-SE, and TS-NE) allowed us to identify the presence of preferential SGD flow paths at the groundwater-seawater mixing zone in the Mobile Bay coastal aquifer (Figs. 6 and S4).

On the western shore, where we found the lowest SGD rates, the sediment core revealed a fine sand layer (C) at a depth of approximately 3.5 m with a hydraulic conductivity (k) of 7.9 m day^{-1} that permitted the groundwater plume to extend up to 80 m. However, above this layer, we identified the presence of a 2.5-m thick silt layer (B) ($k = 4.1$ m day^{-1}) which serves as an aquitard, restricting groundwater flow to Mobile Bay (Figs. 6a and S4a). An independent study conducted recently near our study site TS-W also supports our findings. As part of a local contaminant transport exploration, Beebe and Lowery (2018) also found limited SGD in the western shore with average seepage rates of 4 cm day^{-1} compared to the average 5 cm day^{-1} found in this study. On the southeastern shore, we found that a highly permeable ($k = 22.1$ m day^{-1}) sand layer (D) (Figs. 6b and S4b), which most likely corresponds to the Miocene-Pliocene Aquifer, allowed the groundwater plume to extend up to 70 m offshore. The deep sediment core that we recovered in this area revealed at a depth of 0.5 m an organic fine sand layer (B) ($k = 8.2$ m day^{-1}) that facilitated SGD from the Miocene-Pliocene Aquifer (Fig. 6b), supporting the relatively higher SGD rates we found in this site (Table 2). We suggest that the highest SGD in Mobile Bay, found on the northeastern shore, was a result of the preferential groundwater flow through the coarse sand layer (up to 20-m deep) that was clearly identified by both the ERT images and the sediment core characterization. This top layer has the highest hydraulic conductivity ($k = 58.4$ m day^{-1}) compared to all other sites. However, we found that this coarse sand layer was created artificially to build the numerous beach areas of this section of the bay. This allowed the greatest groundwater plume extension (up to 100 m offshore) and the highest SGD fluxes in Mobile Bay. The ERT images showed that within the first 20 m from the shore, SGD occurs directly from the coarse sand into Mobile Bay while groundwater seepage in the remaining 80 m takes place through the organic fine sand layer (B) (Fig. 6c).

We conclude that the combination of a high hydraulic gradient (0.25%) in the coastal aquifer with the presence of highly permeable sediments ($k = 58.4$ m day^{-1}) facilitated the observed enhanced SGD inputs on the northeastern shore of Mobile Bay (3.9–5.7 × 10^5 m^3 day^{-1}). On the southeastern shore, the presence of the Miocene-Pliocene Aquifer in contact with an organic fine sand with moderate hydraulic conductivity ($k = 8.2$ m day^{-1}) resulted in the second highest SGD fluxes during this study. The absence of coarse beach sand and a lower hydraulic gradient (0.14%) resulted in a slightly lower discharge (2.3–3.8 × 10^5 m^3 day^{-1}) in comparison to the northeastern shore (3.9–5.7 × 10^5 m^3 day^{-1}). In contrast, a low hydraulic gradient (0.07%) and the presence of a silt layer of very low hydraulic conductivity ($k = 4.1$ m day^{-1}) in the western shore determined the lowest SGD inputs (1.8–2.4 × 10^5 m^3 day^{-1}) and highest RSGD (30–56%) component of the research area.

The above-described lithologic heterogeneities in the shallow sediments of Mobile Bay contribute significantly to the large variations in the spatial distribution of SGD. The presence of stratigraphic sequences of sediment layers with varying grain sizes, hydraulic conductivity, and organic matter is common in estuaries worldwide (e.g., Schwartz 2003; Charette 2007; Chin et al. 2010). Estuaries are highly dynamic systems where the sediment transport and deposition dynamics are affected by changing river discharge, predominant winds, tides, and anthropogenic activities (Ridgway and Shimmield 2002; Wilson et al. 2008; Rodriguez et al. 2010; Wang and Andutta 2013). Additionally, most estuaries are the product of the Holocene sea level rise and subsequent river valleys inundation (Dyer 1973; Ridgway and Shimmield 2002). These common processes typically result in analogous lithologic heterogeneity in most estuaries, influencing the presence and magnitude of SGD (e.g., Hwang et al. 2010; Null et al. 2012; Hatje et al. 2017).

Mobile Bay Water Budget

Based on our 3-year investigation, we found that FSGD only represented a maximum of 5% of the total fresh water inputs to the bay during the dry season. During the wet season, FSGD was 5.5 × 10^5 to 11.5 × 10^5 m^3 day^{-1} and the river flow was between 2300 and 2600 × 10^5 m^3 day^{-1}. If we compare these two components, SGD only represented 0.2–0.5% of the total fresh water inputs to the bay during the wet season. However, during the dry season when the river discharge was between 130 and 390 × 10^5 m^3 day^{-1} and FSGD ranged between 2.8 × 10^5 and 6.5 × 10^5 m^3 day^{-1}, FSGD represented 0.7–5.0% of the fresh water inputs to the bay (Table 4, Fig. 8). These estimates of FSGD contribution to the fresh water

budget of Mobile Bay are in close agreement with estimations reported in other river-dominated estuaries worldwide. For instance, Schwartz (2003) found that SGD in the Delaware Estuary accounted on average for 5% of total fresh water discharge. Kim et al. (2010) and Dulaiova et al. (2006) estimated that FSGD represented 3.4 and 4% compared to riverine discharge in the Yeongsan River Estuary (Korea) and the Gulf of Thailand, respectively.

To confirm these findings, in addition to the radioisotope approach, we also used water stable isotopes ($\delta^{18}O$ and $\delta^{2}H$) to evaluate the relative contribution of each of the water sources to Mobile Bay including river and groundwater inputs as well as seawater entrance from Main Pass (Fig. 1). Based on the stable isotope mixing model described in the supplementary material, we found that river inputs dominated the system during the wet season with up to 89% of the total inputs to the bay, whereas seawater entrance in Mobile Bay via Main Pass was 10%. During these periods, FSGD represented only 1% of the water budget (Table 5). Therefore, we suggest that the importance of FSGD is higher during the dry season when river flow decreases significantly. Although the river input is still the dominant source of water to Mobile Bay (61%), the contribution of FSGD is relatively higher, accounting for up to 5% of the water budget. This agrees well with the volumetric comparison between the assessed FSGD and river flow (0.7–5.0%) based on our radioisotope approach. The lower river discharge during the dry season results in a lower flushing rate (from 4.7 km day^{-1} during the wet season to 3.3 km day^{-1}), allowing larger amount of seawater (34%) to enter in the bay via Main Pass (Table 5). Furthermore, the salinity values were significantly higher near Main Pass during the dry season (Figs. S2a and S2b), also supporting this finding.

Although our findings indicate that FSGD is not significant to the water budget of the Mobile Bay as a whole, we found that on a regional scale, SGD appears to be quite important. For instance, we found that FSGD is most important in the northeastern shore where it represented between 26 and 37% of all water inputs when compared to river (50–71%) and seawater inputs (3–14%) (Table 5). Proportionally, FSGD was slightly lower in the southeastern shore, where it represented 30% of the total water inputs during the dry season and 12% during the wet season. River water dominated the system in this area (59–68%), while seawater inputs did not affect this shore significantly (11–20%) due to the counterclockwise water circulation pattern in Mobile Bay (Table 5). With 71–75%, seawater was proportionally the largest component in the water budget of the western shore of Mobile Bay. We found that the fresh water plume from the Mobile-Tensaw River System extending to the south (Figs. S2a and S2b) did not affect significantly the area of the southwestern shoreline (near TS-W) where river inputs represented 11–15% of the total budget. The contribution of FSGD to the budget of the western shore was the lowest of Mobile Bay, representing 10–18% of the total water inputs (Table 5).

Ecological Importance of SGD

During this study, we found that 80% of the total SGD in Mobile Bay occurs preferentially on the east shore, coinciding exactly with the locations most frequently impacted by *Jubilees* as published by Loesch (1960) and May (1973) (Fig. 2). Furthermore, we found that the importance of SGD on the east shore was highest during the dry season (30–36% of the total water inputs), when *Jubilees* and HABs occur (Loesch 1960; Liefer et al. 2009; Mcintyre et al. 2011). We hypothesize that inputs of anoxic SGD drives the water hypoxia that causes *Jubilee*s and could also affect the occurrence of HABs in the east shore of Mobile Bay.

Loesch (1960) showed that *Jubilees* are linked to water hypoxia, which leaves demersal organism in a moribund state. May (1973) further demonstrated that *Jubilees* are triggered by a synergetic combination of physical forces and geochemical reactions that only coincide during the summer months

Table 5 Site- and season-specific values utilized in the $\delta^{18}O$-$\delta^{2}H$ three end-member mixing model to calculate the fractions of riverine, FSGD, and seawater inputs (f_{river}, f_{fsgd}, and f_{ow}) in mobile bay during the dry and wet seasons. The table includes results for water inputs in the whole bay and at each study site individually (TS-W, TS-SE, and TS-NE)

Location	Season	$\delta^{18}O_{River}$ (‰ VSMOW)	$\delta^{18}O_{FSGD}$	$\delta^{18}O_{OW}$	$\delta^{18}O_{MB}$	$\delta^{2}H_{River}$	$\delta^{2}H_{FSGD}$	$\delta^{2}H_{OW}$	$\delta^{2}H_{MB}$	f_{River} (%)	f_{OW}	f_{SGD}
Mobile Bay	Dry	−3.5	−3.6	0.0	−2.3	−18	−19	0	−12	61 ± 7	34 ± 4	5 ± 0.5
	Wet	−3.4	−4.2	0.0	−3.1	−18	−20	0	−16	89 ± 6	10 ± 0.7	1 ± 0.1
TS-W	Dry	−3.0	−3.6	0.0	−1.0	−15	−20	0	−5	11 ± 3	71 ± 21	18 ± 5
	Wet	−4.4	−4.2	0.0	−4.0	−23	−20	0	−22	15 ± 1	75 ± 7	10 ± 1
TS-SE	Dry	−4.0	−3.9	0.0	−2.4	−18	−19	0	−11	59 ± 13	11 ± 2	30 ± 7
	Wet	−4.4	−4.2	0.0	−3.5	−23	−20	0	−18	68 ± 7	20 ± 2	12 ± 1
TS-NE	Dry	−3.0	−3.9	0.0	−2.9	−15	−19	0	−14	50 ± 7	14 ± 2	37 ± 5
	Wet	−4.4	−4.2	0.0	−4.2	−23	−20	0	−22	71 ± 7	3 ± 0.03	26 ± 2

(dry season). When the water column salinity stratification occurs, the bottom water layer remains isolated, favoring biogeochemical oxygen consumption and deriving in water hypoxia (May 1973). These events typically occur at dark during the rising tide with easterly winds below 5 m s^{-1}, minimizing the physical disturbance required for water column mixing (Loesch 1960; May 1973). The easterly wind moves the surface water away from the east shore of the bay while the flooding tide forces the hypoxic bottom water to move towards the shore. Similar to the so-called upwelling, the wind creates a pressure deficiency near the east shore of Mobile Bay that enhances the low-oxygen deeper water to flow with the tide. Turner et al. (1987) and Park et al. (2007) suggested that benthic oxygen demand was the primary cause for the oxygen depletion observed on the east shore of Mobile Bay. However, Cowan et al. (1996) showed that the sediment oxygen consumption on the east shore of Mobile Bay is low compared to other estuaries and could not support hypoxia alone.

We hypothesize that the additional oxygen demand that controls the occurrence of *Jubilees* is supported by inputs of anoxic SGD as it flows through the organic sand layer on the east shore of the bay. The sediment cores collected in the bay showed that the organic sand layer (composed of 36% organic matter) is present only at the intertidal zone of the east shore (Table 1). The ERT images confirmed that SGD occurs through the organic layer on both the southeastern and northeastern shore, extending more than 100 m offshore (Fig. 6). During this study, we observed that groundwater DO was below 1 mg L^{-1} in all intertidal piezometers installed in the organic layer, significantly lower than on the western shore and the inland wells (Fig. 5). We suggest that the abundant organic matter mineralization in the organic layer creates the observed anoxic conditions as SGD occurs through the coastal sediments on the east shore. Evidence to support that the anoxic SGD can directly affect the *Jubilee* events on the east shore is that DO in adjacent bay waters was nearly hypoxic (2.7 mg L^{-1}) during all sampling campaigns (Figs. S1 and 5). Furthermore, there is a clear correlation between the DO in SGD and the DO measured in surface waters of Mobile Bay at each section, indicating that SGD can be causing the oxygen depletion on the east shore (Fig. 5). A similar effect was also observed by Null et al. (2011) in the Neuse River Estuary (North Carolina, USA), where the organic matter degradation in the coastal sediments generated hypoxia in groundwater and ultimately in the estuary surface waters.

Additionally, previous studies have also shown that HABs occur systematically in the southern sector of Mobile Bay during the summer months (Liefer et al. 2009; Mcintyre et al. 2011; Su et al. 2014). Specifically, Liefer et al. (2009) and Mcintyre et al. (2011) associated the occurrence of HABs on the southeastern shore with nutrient inputs delivered by SGD. Although HABs have never been studied in the northeastern shore of the bay, we speculate that the ubiquitous presence of the organic layer on the east shore is an important control on the occurrence of HAB events. The enhanced SGD inputs on the east shore through the organic layer could represent an important source of nutrients to the coastal ecosystem during the dry season, when HABs occur. On the east shore, river inputs are limited and SGD might be the main vector of the excess nutrients required to trigger and support HAB events (Fig. 1).

Conclusions

In this study, we demonstrated that hydrogeological heterogeneities in the shallow sediments controlled the occurrence and magnitude of SGD in Mobile Bay, an estuary historically impacted by *Jubilees* and HABs.

Based on our results, SGD was primarily controlled by marine-driven tidal pumping and represented a maximum of 5.0% of the total fresh water inputs in Mobile Bay during the dry season, when *Jubilees* and HABs occur. We found that SGD occurred preferentially on the east shore of Mobile Bay, accounting for up to 80% of the total SGD in the bay and coinciding exactly with the most frequent areas impacted by *Jubilee* events. We identified that SGD on the east shore occurs through an organic sand layer that creates anoxic conditions in percolating groundwater and adjacent surface water of the bay. We hypothesize that the abundant organic matter decomposition in the organic layer can support the oxygen depletion that drives the *Jubilee* events. Additionally, we speculate that the presence of this organic layer combined with enhanced SGD rates on the east shore could also represent an important source of nutrients to the coastal ecosystem, possibly triggering and supporting HAB events.

Acknowledgements We also want to thank the Mobile District US Army Corps of Engineers, Nathan Coburn, Adam Forkner, Richard Allen, and Steve Dykstra for their extensive help in the field. We are also very grateful for the massive help from the Weeks Bay National Estuarine Research Reserve by providing accommodation and technical support during all field campaigns.

Funding Information This research was partially funded by the National Science Foundation (NSF OIA-1632825), the 2016 ExxonMobil Summer Fund, the 2015 Gulf Coast Association of Geological Societies Student Research Grant, the University of Alabama Graduate School Research and Travel Support Fund, the UA Department of Geological Sciences W. Gary Hooks Geological Sciences Advisory Board Fund, and the A.S. Johnson Travel Fund.

References

Advanced Geosciences, Inc. 2014. Instruction manual for EarthImager 2D, version 2.4.0, Resistivity and IP Inversion Software. (Available at http://www.agiusa.com).

American Association for Testing and Materials. 1993. ASTM D 2974 standard test methods for moisture, ash, and organic matter of peat and organic soils.

American Public Health Association (APHA), American Water Works Association (AWWA), and Water Environment Federation (WEF). 1999. In Standard methods for the examination of water and wastewater 20th Edition, eds. Clescerl L., Greenberg A. and Eaton A. 2–48. United Book Press, Inc., Baltimore, Maryland. Part 2000.

Beebe, D.A., and B.A. Lowery. 2018. Seawater recirculation drives groundwater nutrient loading from a developed estuary shoreline with on-site wastewater treatment systems: Mobile Bay, USA. *Environmental Earth Sciences* 77 (10): 372.

Befus, K.M., M.B. Cardenas, D.R. Tait, and D.V. Erler. 2014. Geoelectrical signals of geologic and hydrologic processes in a fringing reef lagoon setting. *Journal of Hydrology* 517: 508–520.

Bianchi, T.S. 2007. *Biogeochemistry of estuaries*. New York: Oxford University Press.

Bricker, S.B., B. Longstaff, W. Dennison, A. Jones, K. Boicourt, C. Wicks, and J. Woerner. 2008. Effects of nutrient enrichment in the nation's estuaries: A decade of change. *Harmful Algae* 8 (1): 21–32.

Burnett, W.C., and H. Dulaiova. 2003. Estimating the dynamics of groundwater input into the coastal zone via continuous radon-222 measurements. *Journal of Environmental Radioactivity* 69 (1-2): 21–35.

Burnett, W.C., H. Bokuniewicz, M. Huettel, W.S. Moore, and M. Taniguchi. 2003. Groundwater and pore water inputs to the coastal zone. *Biogeochemistry* 66 (1/2): 3–33.

Burnett, W., P. Aggarwal, A. Aureli, H. Bokuniewicz, J. Cable, M. Charette, E. Kontar, S. Krupa, K. Kulkarni, and A. Loveless. 2006. Quantifying submarine groundwater discharge in the coastal zone via multiple methods. *Science of the Total Environment* 367 (2-3): 498–543.

Burnett, W.C., and H. Dulaiova. 2006. Radon as a tracer of submarine groundwater discharge into a boat basin in Donnalucata, Sicily. *Continental Shelf Research* 26 (7): 862–873.

Burnett, W.C., R. Peterson, W.S. Moore, and J. de Oliveira. 2008. Radon and radium isotopes as tracers of submarine groundwater discharge—results from the Ubatuba, Brazil SGD assessment intercomparison. *Estuarine, Coastal and Shelf Science* 76 (3): 501–511.

Byrnes, M., J. Berlinghoff and S. Griffee. 2013. Sediment dynamics in Mobile Bay, Alabama: Development of an operational sediment budget. Applied Coastal Research and Engineering Inc. Mobile Bay National Estuary Program Library, Mobile, AL. (Available at http://www.mobilebaynep.com/library).

Cable, J.E., W.C. Burnett, J.P. Chanton, and G.L. Weatherly. 1996. Estimating groundwater discharge into the northeastern Gulf of Mexico using radon-222. *Earth and Planetary Science Letters* 144 (3-4): 591–604.

Cerdà-Domènech, M., V. Rodellas, A. Folch, and J. Garcia-Orellana. 2017. Constraining the temporal variations of Ra isotopes and Rn in the groundwater end-member: Implications for derived SGD estimates. *Science of the Total Environment* 595: 849–857.

Chandler, R.V., J.D. Moore, and B. Gillett. 1985. Ground-water chemistry and salt-water encroachment, southern Baldwin County, Alabama. *Geological Survey of Alabama Bulletin* 126: 70.

Charette, M.A. 2007. Hydrologic forcing of submarine groundwater discharge: Insight from a seasonal study of radium isotopes in a groundwater-dominated salt marsh estuary. *Limnology and Oceanography* 52 (1): 230–239.

Chin, J.L., D.L. Woodrow, M. McGann, F.L. Wong, T. Fregoso, and B.E. Jaffe. 2010. Estuarine sedimentation, sediment character, and foraminiferal distribution in central San Francisco Bay, California. U.S. *Geological Survey Open-File Report*: 2010–1130.

Cowan, J. L., J. R. Pennock and W. R. Boynton. 1996. Seasonal and interannual patterns of sediment-water nutrient and oxygen fluxes in Mobile Bay, Alabama (USA): regulating factors and ecological significance. *Marine Ecology Progress Series* 141: 229–245.

Craig, H. 1961. Isotopic variations in meteoric waters. *Science* 133 (3465): 1702–1703.

Cross, V.A., J.F. Bratton, K.D. Kroeger, J. Crusius, and C.R. Worley. 2013. *Continuous resistivity profiling data from Great South Bay, Long Island, New York*. U.S. Geological Survey Open-File Report 2011–1040.

Crusius, J., D. Koopmans, J.F. Bratton, M.A. Charette, K.D. Kroeger, P.B. Henderson, L. Ryckman, K. Halloran, and J.A. Colman. 2005. Submarine groundwater discharge to a small estuary estimated from radon and salinity measurements and a box model. *Biogeosciences* 2 (2): 141–157.

Danielson, J.J., J.C. Brock, D.M. Howard, D.B. Gesch, J.M. Bonisteel-Cormier, and L.J. Travers. 2013. Topobathymetric model of Mobile Bay, Alabama. *US Geological Survey Data Series* 769.

Dimova, N., W.C. Burnett, and D. Lane-Smith. 2009. Improved automated analysis of radon (^{222}Rn) and thoron (^{220}Rn) in natural waters. *Environmental Science & Technology* 43 (22): 8599–8603.

Dimova, N.T., P.W. Swarzenski, H. Dulaiova, and C.R. Glenn. 2012. Utilizing multichannel electrical resistivity methods to examine the dynamics of the fresh water–seawater interface in two Hawaiian groundwater systems. *Journal of Geophysical Research: Oceans* 117 (C2).

Dimova, N.T., W.C. Burnett, J.P. Chanton, and J.E. Corbett. 2013. Application of radon-222 to investigate groundwater discharge into small shallow lakes. *Journal of Hydrology* 486: 112–122.

Doctor, D.H., E.C. Alexander, M. Petrič, J. Kogovšek, J. Urbanc, S. Lojen, and W. Stichler. 2006. Quantification of karst aquifer discharge components during storm events through end-member mixing analysis using natural chemistry and stable isotopes as tracers. *Hydrogeology Journal* 14 (7): 1171–1191.

Du, J., K. Park, J. Shen, B. Dzwonkowski, X. Yu, and B.I. Yoon. 2018. Role of baroclinic processes on flushing characteristics in a highly stratified estuarine system, Mobile Bay, Alabama. *Journal of Geophysical Research: Oceans* 123 (7): 4518–4537.

Dulaiova, H., R. Peterson, W.C. Burnett, and D. Lane-Smith. 2005. A multi-detector continuous monitor for assessment of ^{222}Rn in the coastal ocean. *Journal of Radioanalytical and Nuclear Chemistry* 263 (2): 361–365.

Dulaiova, H., W. Burnett, G. Wattayakorn, and P. Sojisuporn. 2006. Are groundwater inputs into river-dominated areas important? The Chao Phraya River—Gulf of Thailand. *Limnology and Oceanography* 51 (5): 2232–2247.

Dulaiova, H., and W.C. Burnett. 2008. Evaluation of the flushing rates of Apalachicola Bay, Florida via natural geochemical tracers. *Marine Chemistry* 109 (3-4): 395–408.

Dyer, K.R. 1973. *Estuaries: A physical introduction*, 140. London: John Wiley & Sons.

Dzwonkowski, B., K. Park, H.K. Ha, W.M. Graham, F.J. Hernandez, and S.P. Powers. 2011. Hydrographic variability on a coastal shelf directly influenced by estuarine outflow. *Continental Shelf Research* 31 (9): 939–950.

Ellis, J. 2013. Evaluation of submarine groundwater discharge and groundwater quality using a novel coupled approach: Isotopic tracer techniques and numerical modeling. Master's thesis, University of Alabama, 67 pp.

Garcia-Solsona, E., J. Garcia-Orellana, P. Masqué, and H. Dulaiova. 2008. Uncertainties associated with ^{223}Ra and ^{224}Ra measurements in water via a Delayed Coincidence Counter (RaDeCC). *Marine Chemistry* 109 (3-4): 198–219.

Garcia-Solsona, E., J. Garcia-Orellana, P. Masqué, V. Rodellas, M. Mejías, B. Ballesteros, and J. Domínguez. 2010. Groundwater and nutrient discharge through karstic coastal springs (Castelló, Spain). *Biogeosciences* 7 (9): 2625–2638.

Geibert, W., V. Rodellas, A. Annett, P. van Beek, J. Garcia-Orellana, Y.T. Hsieh, and P. Masque. 2013. ^{226}Ra determination via the rate of ^{222}Rn ingrowth with the Radium Delayed Coincidence Counter (RaDeCC). *Limnology and Oceanography: Methods* 11: 594–603.

Geological Survey of Alabama. 2018. Assessment of groundwater resources in Alabama, 2010–16. *Geological Survey of Alabama Bulletin* 186: 426.

Gillett, B., D. Raymond, J. Moore, and B. Tew. 2000. Hydrogeology and vulnerability to contamination of major aquifers in Alabama: Area 13. *Geological Survey of Alabama Circular* 199A 68 pp.

Greene, D.L., Jr., A.B. Rodriguez, and J.B. Anderson. 2007. Seaward-branching coastal-plain and piedmont incised-valley systems through multiple sea-level cycles: Late Quaternary examples from Mobile Bay and Mississippi Sound, USA. *Journal of Sedimentary Research* 77 (2): 139–158.

Gu, H., W.S. Moore, L. Zhang, J. Du, and J. Zhang. 2012. Using radium isotopes to estimate the residence time and the contribution of submarine groundwater discharge (SGD) in the Changjiang effluent plume, East China Sea. *Continental Shelf Research* 35: 95–107.

Hatje, V., K.K. Attisano, M.F.L. de Souza, B. Mazzilli, J. de Oliveira, T. de Araújo Mora, and W.C. Burnett. 2017. Applications of radon and radium isotopes to determine submarine groundwater discharge and flushing times in Todos os Santos Bay, Brazil. *Journal of Environmental Radioactivity* 178: 136–146.

Hazen, A. 1893. *Some physical properties of sand and gravels*. Massachusetts State Board of Health. 24th Annual Report.

Henderson, R.D., F.D. Day-Lewis, E. Abarca, C.F. Harvey, H.N. Karam, L. Liu, and J.W. Lane. 2010. Marine electrical resistivity imaging of submarine groundwater discharge: Sensitivity analysis and application in Waquoit Bay, Massachusetts, USA. *Hydrogeology Journal* 18 (1): 173–185.

Holliday, D., T. Stieglitz, P. Ridd, and W. Read. 2007. Geological controls and tidal forcing of submarine groundwater discharge from a confined aquifer in a coastal sand dune system. *Journal of Geophysical Research: Oceans* 112 (C4).

Hwang, D.-W., G. Kim, Y.-W. Lee, and H.-S. Yang. 2005. Estimating submarine inputs of groundwater and nutrients to a coastal bay using radium isotopes. *Marine Chemistry* 96 (1-2): 61–71.

Hwang, D.-W., G. Kim, W.-C. Lee, and H.-T. Oh. 2010. The role of submarine groundwater discharge (SGD) in nutrient budgets of Gamak Bay, a shellfish farming bay, in Korea. *Journal of Sea Research* 64 (3): 224–230.

Johannes, R.E. 1980. The ecological significance of the submarine discharge of groundwater. *Marine Ecology Progress Series* 3: 365–373.

Kim, J., J.-S. Kim, and G. Kim. 2010. Nutrient input from submarine groundwater discharge versus intermittent river-water discharge through an artificial dam in the Yeongsan River estuary, Korea. *Ocean Science Journal* 45 (3): 179–186.

Krantz, D.E., F.T. Manheim, J.F. Bratton, and D.J. Phelan. 2004. Hydrogeologic setting and ground water flow beneath a section of Indian River Bay, Delaware. *Groundwater* 42 (7): 1035–1051.

Lambe, T.W. 1951. *Soil testing for engineers*, 406. New York: John Wiley & Sons.

Lambert, M.J., and W.C. Burnett. 2003. Submarine groundwater discharge estimates at a Florida coastal site based on continuous radon measurements. *Biogeochemistry* 66 (1/2): 55–73.

Lee, D.R. 1977. A device for measuring seepage flux in lakes and estuaries. *Limnology and Oceanography* 22 (1): 140–147.

Liefer, J.D., H.L. MacIntyre, L. Novoveska, W.L. Smith, and C.P. Dorsey. 2009. Temporal and spatial variability in *Pseudo-nitzschia* spp. in Alabama coastal waters: A hot spot linked to submarine groundwater discharge? *Harmful Algae* 8 (5): 706–714.

Loesch, H. 1960. Sporadic mass shoreward migrations of demersal fish and crustaceans in Mobile Bay, Alabama. *Ecology* 41 (2): 292–298.

Null, K.A., D.R. Corbett, D.J. DeMaster, J.M. Burkholder, C.J. Thomas, and R.E. Reed. 2011. Porewater advection of ammonium into the Neuse river estuary, North Carolina, USA. *Estuarine, Coastal and Shelf Science* 95 (2-3): 314–325.

Macintyre, H.L., A.L. Stutes, W.L. Smith, C.P. Dorsey, A. Abraham, and R.W. Dickey. 2011. Environmental correlates of community composition and toxicity during a bloom of *Pseudo-nitzschia* spp. in the northern Gulf of Mexico. *Journal of Plankton Research* 33 (2): 273–295.

May, E.B. 1973. Extensive oxygen depletion in Mobile Bay, Alabama. *Limnology and Oceanography* 18 (3): 353–366.

Michael, H.A., K.C. Scott, M. Koneshloo, X. Yu, M.R. Khan, and K. Li. 2016. Geologic influence on groundwater salinity drives large seawater circulation through the continental shelf. *Geophysical Research Letters* 43 (20): 10,782–10,791.

Montiel, D., N. Dimova, B. Andreo, J. Prieto, J. García-Orellana, and V. Rodellas. 2018. Assessing submarine groundwater discharge (SGD) and nitrate fluxes in highly heterogeneous coastal karst aquifers: Challenges and solutions. *Journal of Hydrology* 557: 222–242.

Moore, W.S. 1976. Sampling ^{228}Ra in the deep ocean. *Deep Sea Research and Oceanographic Abstracts* 23 (7): 647–651.

Moore, W.S., and R. Arnold. 1996. Measurement of ^{223}Ra and ^{224}Ra in coastal waters using a delayed coincidence counter. *Journal of Geophysical Research: Oceans* 101 (C1): 1321–1329.

Moore, W.S. 1996. Large groundwater inputs to coastal waters revealed by ^{226}Ra enrichments. *Nature* 380 (6575): 612–614.

Moore, W.S. 1999. The subterranean estuary: A reaction zone of ground water and sea water. *Marine Chemistry* 65 (1-2): 111–125.

Moore, W.S. 2000. Determining coastal mixing rates using radium isotopes. *Continental Shelf Research* 20 (15): 1993–2007.

Moore, W.S. 2003. Sources and fluxes of submarine groundwater discharge delineated by radium isotopes. *Biogeochemistry* 66 (1/2): 75–93.

Moore, W.S. 2008. Fifteen years experience in measuring ^{224}Ra and ^{223}Ra by delayed-coincidence counting. *Marine Chemistry* 109 (3-4): 188–197.

Moore, W.S., and J. Krest. 2004. Distribution of ^{223}Ra and ^{224}Ra in the plumes of the Mississippi and Atchafalaya Rivers and the Gulf of Mexico. *Marine Chemistry* 864: 105–119.

Moore, W.S. 2010. The effect of submarine groundwater discharge on the ocean. *Annual Review of Marine Science* 2 (1): 59–88.

Noble, M.A., W.W. Schroeder, W.J. Wiseman, H.F. Ryan, and G. Gelfenbaum. 1996. Subtidal circulation patterns in a shallow, highly stratified estuary: Mobile Bay, Alabama. *Journal of Geophysical Research: Oceans* 101 (C11): 25689–25703.

Null, K.A., N.T. Dimova, K.L. Knee, B.K. Esser, P.W. Swarzenski, M.J. Singleton, M. Stacey, and A. Paytan. 2012. Submarine groundwater discharge-derived nutrient loads to San Francisco Bay: Implications to future ecosystem changes. *Estuaries and Coasts* 35 (5): 1299–1315.

Park, K., C.K. Kim, and W.W. Schroeder. 2007. Temporal variability in summertime bottom hypoxia in shallow areas of Mobile Bay, Alabama. *Estuaries and Coasts* 30 (1): 54–65.

Parsons, M.L., and Q. Dortch. 2002. Sedimentological evidence of an increase in *Pseudo-nitzschia* (Bacillariophyceae) abundance in response to coastal eutrophication. *Limnology and Oceanography* 47 (2): 551–558.

Peterson, R.N., W.C. Burnett, M. Taniguchi, J. Chen, I.R. Santos, and T. Ishitobi. 2008. Radon and radium isotope assessment of submarine groundwater discharge in the Yellow River delta, China. *Journal of Geophysical Research: Oceans* 113.

Reed, P.C. 1971. Geologic map of Baldwin County, Alabama. *Geological Survey of Alabama Special Map* 94: 55.

Ridgway, J., and G. Shimmield. 2002. Estuaries as repositories of historical contamination and their impact on shelf seas. *Estuarine, Coastal and Shelf Science* 55 (6): 903–928.

Rodellas, V., J. Garcia-Orellana, G. Trezzi, P. Masqué, T.C. Stieglitz, H. Bokuniewicz, J.K. Cochran, and E. Berdalet. 2017. Using the radium quartet to quantify submarine groundwater discharge and porewater exchange. *Geochimica et Cosmochimica Acta* 196: 58–73.

Rodriguez, A. B., D. L. Greene, J. B. Anderson and A. R. Simms. 2008. Response of Mobile Bay and eastern Mississippi Sound, Alabama, to changes in sediment accommodation and accumulation. In Response of upper Gulf Coast estuaries to Holocene climate change and sea-level rise, eds. J.B. Anderson and A.B. Rodriguez 13–29. Geological Society of America.

Rodriguez, A.B., A.R. Simms, and J.B. Anderson. 2010. Bay-head deltas across the northern Gulf of Mexico back step in response to the 8.2 ka cooling event. *Quaternary Science Reviews* 29 (27-28): 3983–3993.

Roman, C.T., N. Jaworski, F.T. Short, S. Findlay, and R.S. Warren. 2000. Estuaries of the northeastern United States: Habitat and land use signatures. *Estuaries* 23 (6): 743–764.

Russoniello, C.J., C. Fernandez, J.F. Bratton, J.F. Banaszak, D.E. Krantz, A.S. Andres, L.F. Konikow, and H.A. Michael. 2013. Geologic effects on groundwater salinity and discharge into an estuary. *Journal of Hydrology* 498: 1–12.

Santos, I.R.S., W.C. Burnett, J. Chanton, B. Mwashote, I.G. Suryaputra, and T. Dittmar. 2008. Nutrient biogeochemistry in a Gulf of Mexico subterranean estuary and groundwater-derived fluxes to the coastal ocean. *Limnology and Oceanography* 53 (2): 705–718.

Santos, I.R., W.C. Burnett, J. Chanton, N. Dimova, and R.N. Peterson. 2009. Land or ocean?: Assessing the driving forces of submarine groundwater discharge at a coastal site in the Gulf of Mexico. *Journal of Geophysical Research: Oceans* 114 (C4).

Santos, I.R., B.D. Eyre, and M. Huettel. 2012. The driving forces of porewater and groundwater flow in permeable coastal sediments: A review. *Estuarine, Coastal and Shelf Science* 98: 1–15.

Sawyer, A.H., O. Lazareva, K.D. Kroeger, K. Crespo, C.S. Chan, T. Stieglitz, and H.A. Michael. 2014. Stratigraphic controls on fluid and solute fluxes across the sediment–water interface of an estuary. *Limnology and Oceanography* 59 (3): 997–1010.

Schroeder, W.W. 1978. Riverine influence on estuaries: A case study. In *Estuarine interactions*, 347–364.

Schroeder, W.W., S.P. Dinnel, and W.J. Wiseman. 1990. Salinity stratification in a river-dominated estuary. *Estuaries* 13 (2): 145–154.

Schwartz, M. 2003. Significant groundwater input to a coastal plain estuary: Assessment from excess radon. *Estuarine, Coastal and Shelf Science* 56 (1): 31–42.

Stalker, J.C., R.M. Price, and P.K. Swart. 2009. Determining spatial and temporal inputs of freshwater, including submarine groundwater discharge, to a subtropical estuary using geochemical tracers, Biscayne Bay, South Florida. *Estuaries and Coasts* 32 (4): 694–708.

Stieglitz, T.C., P.G. Cook, and W.C. Burnett. 2010. Inferring coastal processes from regional-scale mapping of ^{222}Radon and salinity: Examples from the Great Barrier Reef, Australia. *Journal of Environmental Radioactivity* 101 (7): 544–552.

Stumpf, R.P., G. Gelfenbaum, and J.R. Pennock. 1993. Wind and tidal forcing of a buoyant plume, Mobile Bay, Alabama. *Continental Shelf Research* 13 (11): 1281–1301.

Su, N., W.C. Burnett, H.L. MacIntyre, J.D. Liefer, R.N. Peterson, and R. Viso. 2014. Natural radon and radium isotopes for assessing groundwater discharge into Little Lagoon, AL: Implications for harmful algal blooms. *Estuaries and Coasts* 37 (4): 893–910.

Sun, Y., and T. Torgersen. 1998. The effects of water content and Mn-fiber surface conditions on ^{224}Ra measurement by ^{220}Rn emanation. *Marine Chemistry* 62 (3-4): 299–306.

Tait, D.R., I.R. Santos, D.V. Erler, K.M. Befus, M.B. Cardenas, and B.D. Eyre. 2013. Estimating submarine groundwater discharge in a South Pacific coral reef lagoon using different radioisotope and geophysical approaches. *Marine Chemistry* 156: 49–60.

Taniguchi, M., W.C. Burnett, J.E. Cable, and J.V. Turner. 2002. Investigation of submarine groundwater discharge. *Hydrological Processes* 16 (11): 2115–2129.

Taniguchi, M., T. Ishitobi, and K.I. Saeki. 2005. Evaluation of time-space distributions of submarine ground water discharge. *Groundwater* 43 (3): 336–342.

Tamborski, J.J., A.D. Rogers, H.J. Bokuniewicz, J.K. Cochran, and C.R. Young. 2015. Identification and quantification of diffuse fresh submarine groundwater discharge via airborne thermal infrared remote sensing. *Remote Sensing of Environment* 171: 202–217.

Tovar-Sánchez, A., G. Basterretxea, V. Rodellas, D. Sánchez-Quiles, J. García-Orellana, P. Masqué, A. Jordi, J.M. López, and E. Garcia-Solsona. 2014. Contribution of groundwater discharge to the coastal dissolved nutrients and trace metal concentrations in Majorca Island: Karstic vs detrital systems. *Environmental Science & Technology* 48 (20): 11819–11827.

Turner, R., W. Schroeder, and W.J. Wiseman. 1987. The role of stratification in the deoxygenation of Mobile Bay and adjacent shelf bottom waters. *Estuaries* 10 (1): 13–19.

Uddameri, V., S. Singaraju, and E.A. Hernandez. 2014. Temporal variability of freshwater and pore water recirculation components of submarine groundwater discharges at Baffin Bay, Texas. *Environmental Earth Sciences* 71 (6): 2517–2533.

Walter, G.R., and R.E. Kidd. 1979. *Ground-water management techniques for the control of salt-water encroachment in Gulf Coast aquifers, a summary report*, 84. Geological Survey of Alabama Open-file Report.

Wang, X., and F. Andutta. 2013. Sediment transport dynamics in ports, estuaries and other coastal environments. In *Sediment transport*, ed. A. Manning, 3–35. InTech.

Ward, G.M., P.M. Harris, and A.K. Ward. 2005. Gulf Coast rivers of the southeastern United States. *Rivers of North America*: 125–178.

Webb, B.M., and C. Marr. 2016. Spatial variability of hydrodynamic timescales in a broad and shallow estuary: Mobile Bay, Alabama. *Journal of Coastal Research* 32: 1374–1388.

Wentworth, C.K. 1922. A scale of grade and class terms for clastic sediments. *The Journal of Geology* 30 (5): 377–392.

Wilson, A.M., M. Huettel, and S. Klein. 2008. Grain size and depositional environment as predictors of permeability in coastal marine sands. *Estuarine, Coastal and Shelf Science* 80 (1): 193–199.

Wolfe, D.A., and B. Kjerfve. 1986. Estuarine variability: An overview. In *Estuarine variability*, ed. D.A. Wolfe, 3–17. Academic Press.

Xu, B., W. Burnett, N. Dimova, S. Diao, T. Mi, X. Jiang, and Z. Yu. 2013. Hydrodynamics in the Yellow River Estuary via radium isotopes: Ecological perspectives. *Continental Shelf Research* 66: 19–28.

Young, C., J. Tamborski, and H. Bokuniewicz. 2015. Embayment scale assessment of submarine groundwater discharge nutrient loading and associated land use. *Estuarine, Coastal and Shelf Science* 158: 20–30.

Young, M.B., M.E. Gonneea, D.A. Fong, W.S. Moore, J. Herrera-Silveira, and A. Paytan. 2008. Characterizing sources of groundwater to a tropical coastal lagoon in a karstic area using radium isotopes and water chemistry. *Marine Chemistry* 109 (3-4): 377–394.